Russian Chemical Reviews **73** (9) 899 – 921 (2004) © 2004 Russian Academy of Sciences and Turpion Ltd

DOI 10.1070/RC2004v073n09ABEH000918

Synthesis of functional nanocomposites based on solid-phase nanoreactors

Yu D Tretyakov, A V Lukashin, A A Eliseev

Contents

I.	Introduction	899
II.	Methods for the synthesis of nanomaterials	899
III.	Synthesis of nanoparticles in amorphous matrices	901
IV.	Synthesis of nanoparticles in ordered matrices	901

Abstract. Approaches to the synthesis of functional nanocomposites based on zero-, one- and two-dimensional solid-state nanoreactors formed by zeolite cages, pores of mesoporous matrices, or interlayer cavities in layered compounds are considered. It is demonstrated that the use of solid-state nanoreactors opens up extensive opportunities for designing nanocomposites with specified physicochemical properties and makes it possible to avoid the aggregation of nanoparticles and to protect them from exposure to external factors, thus essentially facilitating the practical utility of these materials. The bibliography includes 304 references.

I. Introduction

The upsurge of interest in nanomaterials and nanotechnologies observed in the past decade manifests itself as a yearly growth (in geometrical progression) in the number of publications on this topic.[1] The unique properties of compounds in the nanocrystalline state [2] made it possible not only to create totally new generations of materials and devices but also to change the fundamental views about the world around us.[3, 4]

The reduction of particles to nanometre sizes changes considerably the properties of materials obtained on this basis, such as the melting point, heat capacity, electric conductance, *etc.*[5, 6] Furthermore, such materials acquire new optical, magnetic and electronic properties.[7, 8] In general, these changes are more prominent the smaller the particle sizes.[9]

The term 'nanoparticle' or 'nanosized particle' has appeared in scientific literature over ten years ago; however, there is no common opinion as to the size below which particles should be considered as nanosized. Quite different definitions of nanosizes can be found in the literature, namely, from a few nanometres to several hundred nanometres.[10] Sometimes, the definition of nanoparticles is related to the emergence of new properties other than the properties of the bulk phase rather than to the particle size.[11] It is believed that the size of nanoparticles is comparable to the correlation radius of some physical phenomenon (*e.g.*, the free-path length of electrons or phonons, the coherence length in a superconductor or the size of a magnetic domain or a solid-phase nucleus).[12] In such case, particles are characterised by quantum-size effects that depend both on the nature of the substance and on its properties. The majority of scientists believe that the maximum size of nanoparticles is 100 nm; however, they do admit that this is a purely arbitrary value, which is only necessary to provide a formal classification.[2, 13]

Two types of nanoparticles are usually distinguished: i, clusters or nanocrystals; and ii, nanoparticles as such. The first type comprises particles with well-defined structures and with sizes of 1 – 5 nm containing up to 1000 atoms, while the second type comprises nanoparticles with sizes of 5 – 100 nm consisting of $10^3 - 10^6$ atoms.[14] However, the latter definition is valid only for isotropic (spherical) nanoparticles, whereas nanowires and layered particles containing many more atoms and having one or two linear dimensions do not satisfy this definition, though they are typical nanoparticles as regards their properties. Owing to such differences in the linear sizes of nanoparticles, it is expedient to subdivide them into one-, two-, and three-dimensional nanoparticles (1D, 2D and 3D, respectively).[11] Lately, a distinction of geometrical and physical dimensionality of nanoparticles appeared.[15] It should be noted that if a nanoparticle has complex shape and structure, it is the size of its structural element rather than the linear size (which can often be much larger than 100 nm) that serves as the characteristic size. Such particles are called nanostructures. They are also subdivided into one-, two- and three-dimensional (zero-dimensional) particles (Fig. 1), depending on the anisotropy of the geometrical elements.

Owing to their unique physicochemical properties, nanoparticles are widely used in the creation of functional nanomaterials; among these, a special role belongs to magnetic and semiconducting nanomaterials due to the exceptional role of the latter in the progress of information technology. For example, superparamagnetic materials based on nanocrystalline transition metals (*e.g.*, Fe, Co and Ni) are used in memory devices with ultra-high data storage density;[16] nanomaterials based on semiconductors (*e.g.*, $A^{II}B^{VI}$ and $A^{IV}B^{VI}$) have unique optical properties and show promise as active elements in lasers with adjustable wavelength, elements of nonlinear optics, and nanoelectronic devices.[17]

II. Methods for the synthesis of nanomaterials

Numerous methods have been developed by now for the synthesis of nanomaterials, both in the form of powders and as inclusions in porous or solid matrices. In this case, ferro- and ferrimagnetics, metals, semiconductors, dielectrics *etc.* can serve as nanophases.

Yu D Tretyakov, A V Lukashin, A A Eliseev Department of Chemistry and Department of Materials Science, M V Lomonosov Moscow State University, Leninskie Gory, 119992 Moscow, Russian Federation.
Fax (7-095) 939 09 98. Tel. (7-095) 939 20 74.
E-mail: yudt@inorg.chem.msu.ru (Yu D Tretyakov).
Tel. (7-095) 939 59 31. E-mail: alex@inorg.chem.msu.ru
(A V Lukashin), eliseev@inorg.chem.msu.ru (A A Eliseev)

Received 9 March 2004
Uspekhi Khimii **73** (9) 974 – 998 (2004); translated by S S Veselyi

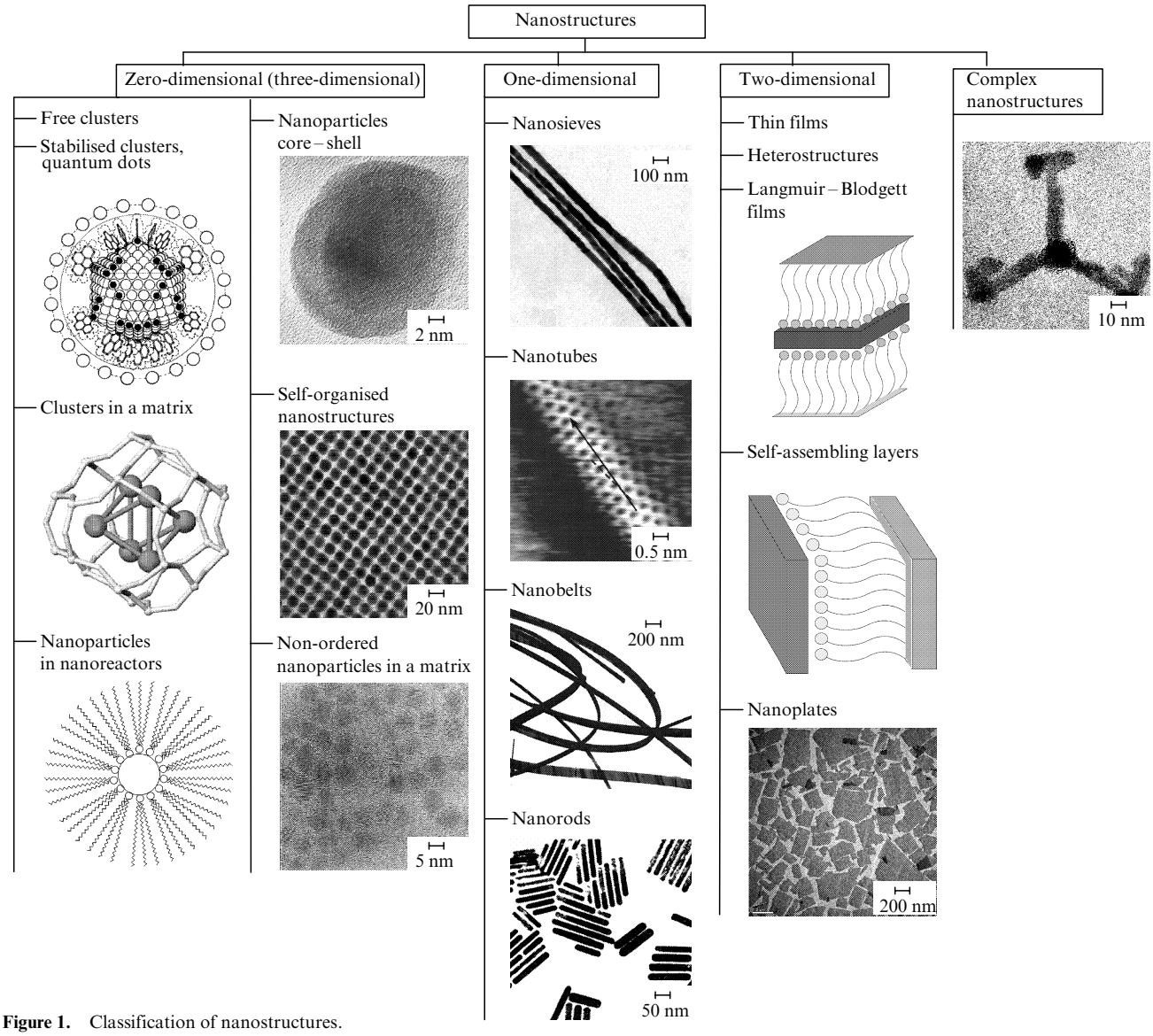


Figure 1. Classification of nanostructures.

According to Fendler,[18] the following conditions are of primary importance in the synthesis of nanomaterials:

1. The systems should be non-equilibrium. Virtually all nanosystems are thermodynamically unstable; they are obtained under conditions that are far from equilibrium, which allows one to achieve spontaneous nucleation and avoid the growth and aggregation of the nanoparticles formed.

2. Uniformity of nanoparticles. The high chemical uniformity of a nanomaterial is ensured if separation of components does not occur during the synthesis, either within a single nanoparticle or between the nanoparticles.

3. Monodispersity of nanoparticles. The properties of nanoparticles depend very strongly on their sizes; therefore, the synthesis of materials with good functional characteristics requires that particles with a sufficiently narrow size distribution be used.

It will be shown below that these conditions are not always mandatory. For example, solutions of surface-active compounds (micellar structures, Langmuir – Blodgett films, liquid – crystal phases) are thermodynamically stable but still give rise to various nanostructures.

All methods for the synthesis of nanomaterials can be tentatively separated into several large groups. The first group includes the so-called high-energy methods based on the rapid condensation of vapours under conditions precluding the aggregation and growth of the particles formed. The methods of this group mostly differ in the techniques of evaporation and stabilisation of the nanoparticles formed. Evaporation can be carried out by means of plasma excitation (plasma-arc), laser radiation (laser ablation), electric arc (carbon arc), or thermal exposure.[19, 20] Condensation was carried out either in the presence of a surfactant that slows down the growth of particles upon adsorption on their surfaces (vapour trapping); or on a cold matrix where the growth of particles is limited by the diffusion rate;[21] or in the presence of an inert component, which allows directed syntheses of nanocomposite materials with various microstructures.[22] If the components are mutually insoluble, the nanoparticle size can be controlled by thermal treatment.[19]

The second group includes mechanochemical methods (ball-milling), which make it possible to obtain nanocomposites by milling together mutually insoluble components in planetary mills or by decomposition of solid solutions to give new phases under exposure to mechanical stress.[23]

The third group of methods is based on the formation of spatially confined systems, that is, nanoreactors (micelles, droplets, films, *etc.*).[24–26] They also include synthesis in reverse micelles,[27] in Langmuir – Blodgett films[28] and in adsorbed layers.[29] Obviously, the size of the particles formed in this case cannot exceed the size of the corresponding nanoreactor,[30] hence these methods make it possible to obtain monodisperse systems. The biomimetic[31] and biological methods for nanoparticle syn-

thesis, where biomolecules (proteins, DNA, *etc.*) serve as nanoreactors, can also be attributed to this group.

The fourth group includes the methods based on the formation of ultramicrodisperse colloidal particles in solutions by polycondensation in the presence of surfactants that prevent aggregation.[32]

The fifth group comprises chemical methods for the synthesis of highly-porous and finely-dispersed structures (Rieke metals, Raney nickel) based on the removal of one component from a microheterogeneous system as a result of a chemical reaction or anodic dissolution. The traditional synthesis of nanocomposites by quenching a glass or salt matrix with a dissolved compound, which results in crystallisation of this compound in the matrix (glasses modified by semiconducting or metallic nanoparticles)[33] can also be classified as such a method. In this case, a compound can be introduced in a matrix in two ways: by adding it to a melt (solution) followed by quenching or by direct introduction into a solid matrix using ion implantation.[34]

Sol–gel synthesis is among the most widespread chemical methods for the synthesis of nanomaterials. It is used to obtain homogeneous oxide systems; chemical modifications of the latter (reduction, sulfidising, *etc.*) gives nanoparticles of the corresponding material in a matrix.[35–39] It should be noted that the sol–gel method makes it possible to obtain nanomaterials with improved functional properties by monitoring the composition and structure of the intermediate products.[40–42] It is also attractive because it can be implemented under laboratory conditions.[24] However, this method suffers considerable drawbacks. First, it does not ensure the formation of monodisperse particles. Second, it does not allow one to obtain anisotropic systems that can be synthesised in nanoreactors, such as two- and one-dimensional nanostructures as well as spatially ordered structures consisting of nanoparticles arranged at equal distances from each other or of parallel nanoplates interlaid with an inert matrix. Finally, in certain cases the required nanocomposite cannot be obtained due to the chemical reaction of particles with a gel-forming agent.

It should be noted that the use of free nanoparticles and nanostructures as materials is quite difficult due to the metastability of compounds in the nanocrystalline state. As noted above, this is caused by an increase in the specific surface of particles with a decrease in their linear dimensions to nanometres resulting in an increase in the chemical reactivity of a compound and in the enhancement of aggregation processes. In order to prevent the aggregation of nanoparticles and to protect them from external factors (*e.g.*, oxidation by atmospheric oxygen), nanoparticles are enclosed in a chemically inert matrix.[43]

Analysis of literature data shows that dozens of methods for matrix isolation of nanostructures have already been developed; these can be arbitrarily separated into two groups: i, synthesis of free nanoparticles followed by incorporation into an inert matrix and ii, direct formation of nanostructures in the bulk of a matrix in the course of its chemical modification.[12,44]

The first group of methods is easy to implement but the choice of the matrices is limited considerably. As a rule, polymeric organic compounds that do not have very high thermal stability and do not always have the required physical properties (*e.g.*, high optical transparency) are used as the matrices.[45] Furthermore, aggregation of nanoparticles during the incorporation cannot be prevented.[46]

The second group of methods makes it possible not only to avoid these drawbacks but also to directly monitor the parameters of nanoparticles in a matrix during the stage of their formation and even to change these parameters during the exploitation of a material. Matrices used for these purposes should contain structural cavities that can be occupied by compounds, subsequent modification of which would result in the formation of nanoparticles in these cavities.[47] In other words, these cavities should confine the zone of a reaction involving the compounds incorporated in them, *i.e.*, serve as specific nanoreactors. Obviously, it is possible to synthesise nanostructures with different morphology and anisotropy by choosing compounds with different shapes of their structural cavities.

The syntheses of nanomaterials with the use of porous oxide matrices (usually SiO_2 or Al_2O_3)[48,49] can serve as examples. However, due to the disordering of the porous structure of such matrices and the rather wide pore size distribution, it is almost impossible to obtain satisfactorily formed nanosystems by this method. Nanocomposites obtained in porous oxide matrices are usually employed in catalysis where the requirements for the monodispersity of particles are not too high.[50] Moreover, the rigid porous structures of such matrices do not allow the size and morphology of particles to be changed during the synthesis; as a rule, the latter parameters depend very strictly on the pore size and morphology,[51] that is, a very limited range of nanostructures can be obtained in a single type of matrix.

Sometimes, fast directed formation of nanoparticles in a matrix is achieved using additional physical effects, such as ultrasonic treatment as well as microwave and laser irradiation.[52–54]

III. Synthesis of nanoparticles in amorphous matrices

The first practical experience in obtaining nanoparticles in amorphous matrices, *viz.*, the preparation of coloured glass, dates back to the age of ancient Egypt.[4] However, the mechanism of colouring in such amorphous matrices was established only 100 years ago.[55] At present, crystallisation of glass is the main method for the synthesis of nanoparticles in amorphous matrices. It is known that the nucleation and growth of crystals in an amorphous matrix depend both on the heat treatment conditions of a glass and on its composition. The crystal size can be controlled by creating a certain concentration of nuclei, which is achieved by heat treatment of a glass at a relatively low temperature. The subsequent growth of crystals occurs at the higher temperature of annealing. It should be noted that the matrix composition changes during the crystallisation and hence the diffusion mobility of ions that constitute the crystalline phase also changes (decrease in the diffusion coefficient slows down the growth of particles and favours the formation of smaller particles of the disperse phase, whereas an increase in the diffusion coefficient favours the formation of larger particles).

Glass crystallisation has been used to obtain diverse nanoparticles of semiconducting, magnetic and catalytically active materials.[56–59] In particular, glasses doped with nanoparticles of semiconductors are widely used as optical filters. In the first place, they are attractive owing to their nonlinear optical properties, such as a considerable resonance effect, a dependence of the position of the absorption edge on the particle size, the doubling of the incident radiation frequency (generation of the second harmonic), *etc.*[60] The possibility of utilising glasses containing nanoparticles of high-coercivity magnetic phases (barium and strontium hexaferrites) as a medium for data recording and storage was considered.[61–68]

However, the glass crystallisation method does not provide nanoparticles with a sufficiently narrow size distribution, which is necessary for the manifestation of the quantum confinement effects or for the utilisation of such nanoparticles in technology.[66] This problem is solved by using porous materials with ordered pore structures, such as mesoporous silica and zeolites having one-dimensional channels or two-dimensional cavities.[67–69] It these cases, nanoparticles of filiform, layered or spherical shapes (depending on the type of the porous structure) with narrow size distributions were obtained.[67,70,71]

IV. Synthesis of nanoparticles in ordered matrices

Ordered matrices (or nanoreactors) are usually classified in accordance with the dimensionality of the pores they contain. Let us successively consider the synthesis of nanoparticles in zero-, one- and two-dimensional nanoreactors.

1. Synthesis of nanoparticles in zero-dimensional nanoreactors

Zero-dimensional nanoreactors are materials characterised by open porosity with an ordered arrangement of spherical pores. Such materials primarily include zeolites, *i.e.*, natural and synthetic aluminosilicates with the composition $M^{i}_{x}M^{ii}_{y}(Al_{x+2y}Si_{z}O_{2x+4y+2z})\cdot n\,H_2O$.[72] More than 150 types of zeolites, including about 30 natural ones, are known to date. Zeolite structures are built of $[SiO_4]^{4-}$ and $[AlO_4]^{5-}$ tetrahedra connected by common vertices into a three-dimensional framework penetrated by cavities and channels where water molecules and cations of alkaline (M^{i}) and alkaline-earth metals (M^{ii}) are located.

Unlike the framework atoms bound by covalent bonds, the cations located in the channels are bound with a matrix only electrostatically and can easily be exchanged for other cations in aqueous solutions.

Isomorphous replacement of aluminium atoms belonging to the framework by atoms of other elements, such as B, Ga, Fe, Co, Ti, or V, and exchange of cations incorporated in the pores allow one to modify the properties of zeolites in a desired direction. There are several factors that determine the possibility of isostructural replacement:[73]

— the similarity of the radii of the replaced and replacing atoms (the larger the difference in the radii the less energetically favourable the replacement);

— the replacement of a smaller atom by a larger one is possible provided that the coordination of the latter is smaller, and *vice versa*;

— the similarity of the electronegativities and ionisation potentials of the replaced and replacing atoms;

— the achievement of the minimum free energy during isomorphous replacement with retention of the coordination number.

The structures of zeolites are more open than those of other tectosilicates. The TO_4 tetrahedra (primary assembly units) form rings of various sizes and the rings are connected to give more complex structures (secondary assembly units). Each type of zeolites is characterised by a definite set of secondary assembly units. [It should be noted that the Si—O—Si angle can vary in rather a wide range (135–165°); as a result, the existence of silicon–oxygen rings with different numbers of atoms becomes possible.] Rings with five oxygen atoms, in which the Si—O—Si angle is about 145°, are more typical of zeolites with a high silicon content. Zeolites with a high aluminium content, which incorporate many Si—O—Al bonds, are mostly built of rings containing three or six oxygen atoms. The structures of natural zeolites most often contain rings with four or six oxygen atoms.

The classification of zeolites is rather a complex task. Each individual structure is described by the structural code comprising three Latin letters, *viz.*, the so-called IZA-code accepted by the International Zeolite Association Structure Commission (http://www.iza-structure.org/databases/). This code is applicable both to aluminosilicates and to some other compounds with similar structures containing atoms of elements (Si, Al, P, Ga, Ge, B, Be, *etc.*) in a tetrahedral environment.

The most general approach to the synthesis of zeolites is based on the joint hydrolysis of silicon compounds and compounds of a three-charged metal (most commonly aluminium) in the presence of an alkali and a quaternary amine (template). Organosilicon compounds that readily undergo hydrolysis, sodium silicate and silica gel with large surface area ($>200\ m^2\ g^{-1}$) are the most common sources of silicon atoms, whereas metal salts (sulfates, nitrates or chlorides) or alkoxides (isopropoxides, butoxides) are most commonly used as the sources of M^{3+} ions.

The schemes for the synthesis of zeolites with different compositions and structures are almost the same. The gels containing silicon and aluminium compounds are aged for prolonged periods of time below the crystallisation temperature (often under hydrothermal conditions) in the presence of templates. This time is necessary for a zeolite with a required structure to be formed in a high yield. The aging conditions and the nature of the templates play a decisive role in the structures of the zeolites formed.[74] The presence of template molecules increases the crystallinity of the aluminosilicate framework and affects its structure. Zeolites of some structural types can also be formed without a template. The structural type of the resulting zeolite also depends on the nature and concentration of the source of the three-charged metal.

The negative charge of the matrix in a zeolite is compensated by ions of alkaline metals, ammonium and/or alkylammonium (depending on the reagents used in the synthesis). Metal cations are generally removed by washing or by ion exchange for NH_4^+, since the presence of metal cations decreases the thermal stability of the matrices obtained. In order to remove the template, the ready zeolites are burnt off in a stream of oxygen at 500–550 °C, which converts them into the so-called H-form. The Si : Al ratio in zeolites is determined by standard methods of quantitative analysis.

Zeolites and similar porous materials are used as ion exchangers, selective adsorbents, catalysts and catalyst supports. The preparation of nanocomposite materials for catalytic purposes (isomerisation of aromatic hydrocarbons, treatment of NO and NO_2 gases) based on zeolites is a promising field of application of zeolites, hence it is not surprising that the majority of works in this field deal with the synthesis of nanoparticles of metals belonging to the 8–11th groups of the Periodic system. Zeolites of the FAU, LTA, SOD and MFI types are most commonly used as the matrices due to their accessibility and the facility of synthesis.[75–82] It should be noted that these matrices have a number of unique properties that are important for the directed synthesis of nanomaterials. Their structures are stable over a broad temperature range. The number of cations in the pores determined by the Al : Si ratio can be easily controlled during the synthesis, which allows one to vary the concentration of the reaction centres in the matrix.

Due to the open porosity of zeolites and the high diffusion rate of gases in the pores, chemical reactions involving intercalated cations can be carried out at elevated temperatures (*e.g.*, reduction with hydrogen required for the preparation of magnetic nanocomposites) almost without destruction of the matrix that confines the reaction zone. These properties open up rich possibilities for the chemical design of nanocomposite materials based on zeolites.

Nanomaterials based on zeolite Y (FAU type) are the most popular.[76, 77, 79–85] The structure of a Y-zeolite consists of the following secondary assembly units: 6-6 (hexagonal prism), 6-2 (hexagon and square with a common edge), 6 (hexagon) and 4 (square) (Fig. 2). The main structural motif of FAU zeolites consists of an octahedron truncated by a cube, *i.e.*, a sodalite cell or a small β-cage with an internal diameter of 0.66 nm comprising four-membered (the free diameter is less than 0.1 nm) and six-membered rings (the diameter is ~0.22 nm) from T-atoms. The vertices of the polyhedron contain 24 T-atoms, whereas the oxygen atoms are located between them. Connection of such polyhedrons through hexagonal prisms (cage diameter 0.36 nm) consisting of T- atoms gives the structures of zeolites (X and Y). They are charactised by a cubic symmetry (*Fm*3*m*) with lattice parameters of $a = 24.345$ Å (Fig. 3). The structure contains different types of cages: the α-cage (supercage) is the largest (its diameter is 1.2 nm) and is surrounded by eight truncated octahedrons; the β-cage (sodalite cage) is limited by a truncated octahedron; and the γ-cage is a hexagonal prism (see Fig. 2).

The main method for the preparation of nanocomposite materials based on zeolites involves the exchange of Na^+, H^+ and NH_4^+ cations contained in zeolites for cations of other metals in aqueous solutions followed by the reduction of the metal with hydrogen. For example, the preparation of a copper-containing zeolite by ion exchange of copper nitrate with a NaY-zeolite or by annealing a mixture of a NaY-zeolite with copper chloride at 420 °C was reported.[86] In the case of solid-phase annealing, the starting zeolite NaY was first stabilised by adding NaBr in order

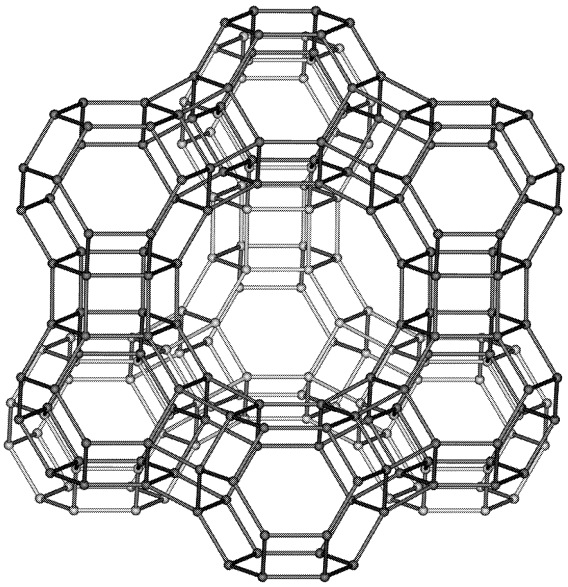


Figure 2. Structure of zeolite Y.

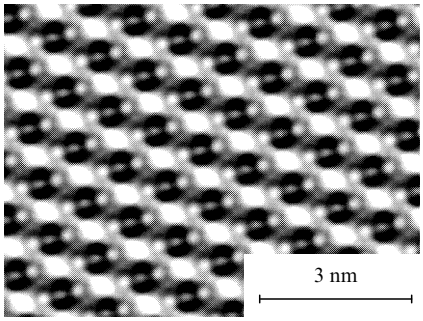


Figure 3. A photomicrograph of a NaY crystal along the [110] direction obtained by transmission electron microscopy (TEM).[76]

to fill the β-cages. This made it possible to introduce copper into α-cages and to increase the thermal stability of matrices. The reduction was carried out in a hydrogen atmosphere at temperatures of 300 – 600 °C. In both cases, the resulting copper particles (3 – 7 nm) were larger than the α-cages and the porous structure of the zeolite was damaged.

Au/NaY and Au-Fe/NaY nanocomposites were obtained in a similar way.[79, 82] Again, the nanoparticles resulting from the reduction of the metals were much larger than the size of the zeolite's α-cage.

Lanthanide-containing zeolites of the FAU structural type are formed upon ionic exchange of cations within zeolites with chlorides or nitrates of rare-earth metals.[83] Annealing at 500 °C of zeolites modified by this method gives oxides of rare-earth metals and results in a partial replacement of aluminium atoms in the zeolite structure by rare-earth atoms, which improves the thermal stability of the zeolite. At sufficiently high concentrations of lanthanides, their oxides are also formed outside the zeolite.

Aside from metal salts, complex cations can also be used. For example, the $Pd(NH_3)_4Cl_2$ complex was used[87] to obtain a palladium-containing zeolite. A Y-zeolite was soaked with a solution of the complex, annealed at 500 °C in a stream of oxygen and reduced with hydrogen at 400 °C. Samples with an overall palladium content from 1% to 10% were obtained using this method; at high palladium concentrations, the size of the nanoparticles that formed exceeded the size of the Y-zeolite cavity, which resulted in the destruction of the porous structure. In contrast, the sample containing 1% of palladium retained the structure of the original zeolite and its pores contained palladium particles with sizes about 1 nm.

Guillemot *et al.*[80] described the synthesis of gold nanoparticles with diameters of ~2 nm in a Y-zeolite matrix by soaking the zeolite with the $Au(en)_2Cl_3$ complex (en is ethylenediamine) followed by decomposing the complex at 250 °C in a stream of helium. According to X-ray photoelectron spectroscopy (XPS), the particles of gold occupied the α-cages of the zeolite.

Publications on the synthesis of nanoparticles of intermetallides† using zeolites have recently appeared. This method was used to obtain (Pt, Pd)-substituted zeolites.[88] Ammonia complexes of palladium and platinum were incorporated in a Y-zeolite by ion exchange. Thermolysis of metal complexes in a stream of oxygen at 300 °C followed by reduction in a stream of hydrogen at 300 °C produced nanoparticles of an alloy containing ~40% of platinum; however, data about the arrangement of the nanoparticles in the zeolite matrix are not available.

An Au – Pd intermetallide was obtained in a Y-zeolite using the $[Au(en)_2]^{3+}$ complex as the source of gold and $Pd(NH_3)_4^{2+}$ as the source of palladium.[89] Ion exchange was carried out in two stages. In the first stage, the palladium complex was introduced in the zeolite matrix; thermolysis of this complex in oxygen was accompanied by the formation of Pd atoms and their transfer to β-cages that are more favourable in terms of coordination. After that, ion exchange with the gold complex and reduction of the composite were carried out. The alloy was formed in the α-cage of the zeolite. Depending on the Au : Pd ratio and the composition of the starting zeolite, particles with sizes from 1 to 3 nm were obtained. Prolonged annealing resulted in the melting of the nanoparticles and their simultaneous growth (to 3.5 – 4 nm) as well as in a partial destruction of the porous structure of the zeolite.

Lázaro *et al.*[78] suggested a very interesting approach to the synthesis of clusters in zeolite cages based on the incorporation of hydrophobic compounds. Iron pentacarbonyl was used as the starting hydrophobic compound due to its ability to form iron clusters upon decomposition *in vacuo*; a dehydrated FAU-zeolite was used as the zeolite. Homogeneous incorporation of the carbonyl into the structure of the dehydrated zeolite could be expected, since the absence of internal OH groups on the cage walls makes their surfaces close to hydrophobic. In order to synthesise nanoparticles, a dehydrated NaY-zeolite was first soaked with iron pentacarbonyl at 77 °C and the pentacarbonyl was then thermally decomposed in a high vacuum. This resulted in superparamagnetic iron clusters with particle sizes from 1.5 to 2.0 nm (according to data from Mössbauer spectroscopy, more than 90% of the iron in the zeolite existed in the metallic state). Clusters were formed in pores, and the zeolite structure was not destroyed.

Carlsson *et al.*[76] studied the arrangement of iron oxide clusters in a Y-zeolite. The clusters were obtained by oxidation of iron pentacarbonyl in the matrix at low temperatures.[90] According to chemical analysis and electron diffraction data, the composition of iron oxide clusters is Fe_6O_n. The clusters are arranged in the β-cavities of the zeolite (Fig. 4); they are octahedra of iron atoms with a distance of 3.6 ± 0.15 Å between the latter. There are 76 $FeO_{1.5}$ units per unit cell of the zeolite.

It should be noted that the synthesis of nanocomposites in zeolites is not limited to matrices of the FAU structural type. There are a fair number of works dealing with the synthesis of nanocomposites in zeolites of the MFI structural type (as well as of the ZSM, MAS and other types) that correspond to one-dimensional nanoreactors.

An unconventional physical approach to the intercalation of chemical compounds into a zeolite matrix is described in a series of

† Nanoparticles of intermetallides are usually obtained by the substitution of ions in solutions containing either both cations or cationic complexes in the required ratio.

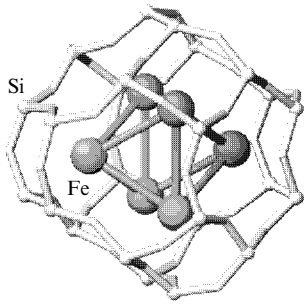


Figure 4. Schematic representation of a cluster in the β-cage of a Y-zeolite.[76]

works.[75, 91, 92]. Au_2Cl_6 was incorporated in dehydrated NaY through the gas phase in a high vacuum and then the gold was reduced to the 1+ oxidation state. As a result, AuCl clusters were formed in the zeolite pores.

It was also found to be rather promising to obtain functional optical materials based on nanoparticles of binary compounds in zeolite matrices. In such materials, it was possible to combine the properties of free nanoparticles with the solid-phase properties of the matrix. It should be noted that the open porosity of the zeolite matrix usually simplifies the reactions of compounds intercalated in it with gaseous reagents. For example, Garcia *et al.*[93] described a procedure for the preparation of a CdS/mordenite (MOR) composite. To do so, the starting zeolite $Na_8[Al_8Si_{40}O_{96}] \cdot 24\,H_2O$ (mordenite with a two-dimensional system of channels 0.65×0.70 nm and 0.26×0.57 nm) was treated with a cadmium nitrate solution, and sulfidised in a stream of hydrogen sulfide. The resulting nanocomposite contained cadmium sulfide particles with a diameter of ~60 nm that were much larger than the pore size. Although the zeolite lost crystallinity, the resulting nanocomposite partially retained the structural elements corresponding to the original mordenite structure. A NiS/Y nanocomposite was obtained in a similar way.[85] An NaY zeolite was placed in a $NiCl_2$ solution, dried (He, 400 °C, 2 h) and sulfidised (10% H_2S/H_2, 2 h) at different temperatures ($T = 25-400$ °C). In this case, the formation of large sulfide particles was observed as well.

A more successful example of using zeolites as nanoreactors is described in Ref. 84. Mixed sulfides of cobalt and molybdenum in a Y-zeolite were obtained by successive replacement of Na^+ ions by cobalt ions followed by incorporation of molybdenum hexacarbonyl into the zeolite in a stream of CO. According to chemical analysis, there are about two $Mo(CO)_6$ molecules per α-cage of the zeolite. The overall composition of the sample obtained at this stage is described by the formula Co(4 mass %)Mo(10 mass %)NaY. After that, the sample was sulfidised in a stream of H_2S at different temperatures (25–400 °C). The sizes of the resulting particles of mixed sulfides were 1–2 nm.

Zeolites are also widely employed as matrices for the synthesis of luminescent nanoparticles.[94]

At present, the complexity of studying the distribution of nanoparticles in a matrix by direct observation methods, such as transmission electron microscopy (TEM), is the main problem in the preparation of nanocomposites based on zeolites. Therefore, syntheses of nanocomposites isolated in matrices are most commonly based on matrices with ordered porous structures and with pore sizes of 2–50 nm. Such matrices include mesoporous molecular sieves and porous alumina.

2. Synthesis of nanoparticles in one-dimensional nanoreactors

The scope of materials that can be used as one-dimensional solid-state nanoreactors is not vast. It includes MFI-type zeolites, mesoporous molecular sieves and mesoporous structures based on alumina.

a. Zeolites of the MFI structural type

MFI type zeolites have an ordered system of channels with diameters ranging within 0.54–0.56 nm and with hexagonal packing (Fig. 5).[74, 95–100] Metal nanoparticles in channels of MFI-zeolites are usually obtained by ion exchange of protons (zeolite in the H^+-form) for metal cations or complexes followed by mild reduction in a stream of hydrogen.

It should be expected that the reduction of metal cations in the matrices of such zeolites would produce anisotropic nanoparticles (unfortunately, the size distribution of particles and their anisotropy were not studied due to the difficulties resulting from the small sizes of the channels).

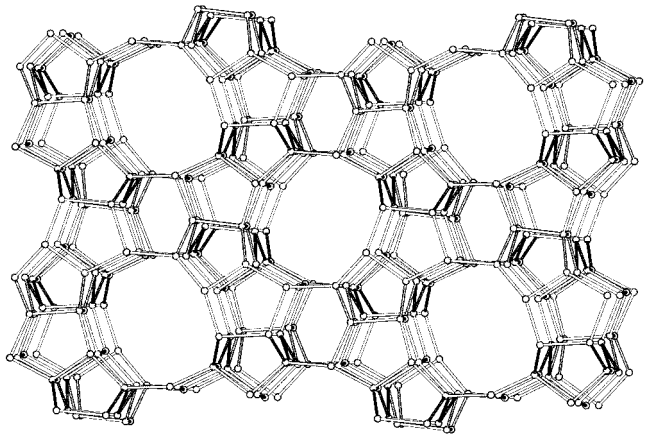


Figure 5. Structure of a zeolite with the MFI structural type.

b. Mesoporous molecular sieves

Mesoporous molecular sieves have been discovered by researchers of the Mobile Research and Development Corporation (USA) in 1992.[101] They synthesised a family of SiO_2-based molecular sieves (MCM-41) with a uniform and highly ordered distribution of pores, the size of which could be strictly controlled in the range from 2 to 10 nm, and with an extremely large specific surface area (~1000 $m^2\ g^{-1}$).

The template method is the most popular method for synthesising mesoporous SiO_2. A template is a centre around which the main structural units of a matrix are arranged and its framework is formed. Removal of a template produces a cavity with the same size and shape as those of the template. The accuracy of the 'printout' after the removal of the template depends on several factors: the nature of the template–matrix interaction, the ability of the matrix to assume the outlines of the template, the relative size of the template and the structural units of the matrix. The scheme of template synthesis is shown in Fig. 6.

Although the discovery of molecular sieves dates back to 1992, a 'template synthesis' was first described in 1949 in a study of gel formation by tetraethoxysilane (TEOS) in the presence of the methyl orange indicator (template). The silica gel formed upon condensation of TEOS selectively adsorbed methyl orange. Since that time, this rather simple and elegant method has become popular for the synthesis of numerous organic and inorganic materials.[30]

Let us consider the synthesis of molecular sieves for mesoporous SiO_2 (MCM) as an example. Samples of MCM are obtained by the polycondensation of silicon compounds [$Si(OMe)_4$ or $Si(OEt)_4$] in the presence of a template. Various molecules can serve as the template,[101–106] *e.g.*, noncovalently bound organic surfactants [as a rule, cetyltrimethylammonium bromide ($C_{16}H_{33}NMe_3Br$) is used].

Bifunctional molecules of cetyltrimethylammonium bromide are amphiphilic, *i.e.*, they contain a hydrophilic head group and a hydrophobic 'tail'. In aqueous solution, such molecules combine

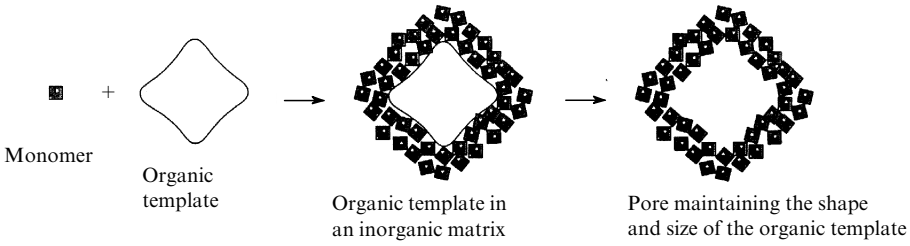


Figure 6. Scheme of template synthesis.

into micelles, in which the hydrophilic head groups form the external surface, whereas the hydrophobic 'tails' are oriented towards the centre. The extent of micellisation and the shape of micelles depend on the surfactant concentration. At high surfactant concentrations, micelles are aggregated into liquid-crystal phases the structure of which depends on the solution temperature and concentration. Figure 7 shows the phase diagram of the $H_2O-C_{16}H_{33}NMe_3Br$ system.[30]

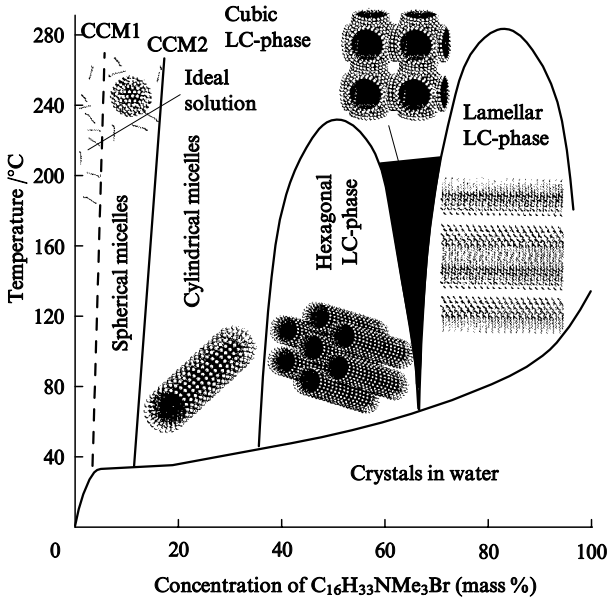


Figure 7. Schematic phase diagram of the $C_{16}H_{33}NMe_3Br-H_2O$ system (LC phase designates the liquid-crystal phase).[30]

A reaction mixture containing an aqueous solution of the surfactant, a tetraalkoxysilane and an acid (or alkali) is kept for a few hours at a constant temperature (80 °C). Hydrolysis of the tetraalkoxysilane produces mesoporous silica around the surfactant micelles.

Parameters affecting the gel formation include the pH of the solution, the nature and concentrations of the template and the organosilicon compound, the temperature, the type of the catalyst, *etc.*[103] Particular importance is attributed to the pH of the medium, more exactly, the ζ-potential that characterises the electrostatic interaction between the colloid particles and determines the structure of the polycondensation products. In the case of acid catalysis, the hydrolysis of a tetraalkoxysilane is probably the limiting step, whereas the condensation is relatively fast. As a result, weakly branched sol particles are formed.

Different types of template–matrix binding are possible. In our case, the template–matrix interaction occurs due to electrostatic forces, hydrogen bonds or van der Waals bonds.

Sodium silicate is sometimes used as the source of silicon.[105, 107] The types of mesoporous phases obtained by the method described are presented in Table 1 and in Fig. 8.

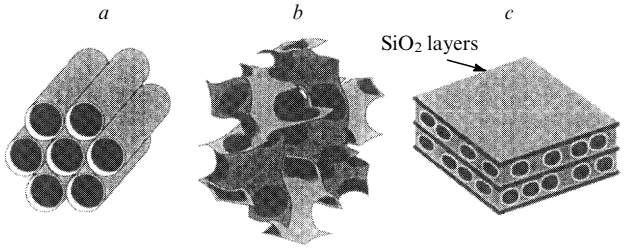


Figure 8. Possible structures of MCM-phases.[112] (*a*) hexagonal, (*b*) cubic, (*c*) lamellar.

Hydrothermal synthesis is an alternative method for the synthesis of mesoporous silica. A reaction mixture containing an aqueous solution of a surfactant and amorphous silica is subjected to prolonged hydrothermal treatment at about 150 °C. Such treatment results in the dissolution of silica accompanied by the rearrangement of its structure. Hydrolysed silicon oxide forms mesophases around the surfactant micelles.[113]

In the syntheses of MCM-41, the surfactant concentration in the starting solution is nearly always maintained below the critical micelle concentration (CMC1) (see Fig. 7), *i.e.*, the liquid-crystal phase is absent in the solution before the addition of a silicon source. This means that SiO_2 and a surfactant are mutually assembled into an organic–inorganic liquid-crystal phase during the reaction. It is assumed that ion exchange of the surfactant with multiply charged oligomeric silicate ions is the first step of the

Table 1. Types of mesoporous SiO_2 phases obtained by the template method.

Type of mesoporous SiO_2 phase	Template	Pore structure	Pore diameter /nm	Ref.
MCM-41	$C_nH_{2n+1}N^+Me_3X^-$ ($n = 6-22$, X = Hal, OH)	hexagonal (Fig. 8 *a*)	2–10	101
MCM-48	the same	cubic (Fig. 8 *b*)	2–5	108
MCM-50	"	lamellar (Fig. 8 *c*)	4	109
BSA-15	triblock-copolymers	hexagonal	5–30	104
MSU-V	$H_2N(CH_2)_nNH_2$ ($n = 12-22$)	hierarchic lamellar	1.3–2.7	110
MAS-5	$C_{16}H_{33}N^+Me_3Br^-$	hexagonal	3	111

formation of mesoporous materials if charged surfactants are used. Silicate ions are polydentate and can bind several surfactant molecules by shielding the repulsion forces between the head groups of the surfactant molecules, thus allowing micelles to increase in size. This effect is well known for simple surfactant–water systems. For example, the addition of electrolytes to $C_{16}H_{33}NMe_3Br$ solutions results in a transition from spherical to cylindrical micelles.[114] Hence, the interaction of surfactant micelles with silicate polyanions produces micellar rods encapsulated in silicate, which then spontaneously build a hexagonal structure.

It should be noted that this mechanism does not operate if neutral surfactants are used as templates. They have a much stronger tendency to form aggregates in water than charged surfactants (the CMC values for charged surfactants are about two orders higher than those of neutral surfactants with the same number of carbon atoms in the alkyl chain). The tendency of neutral surfactants towards aggregation combined with their tendency towards interaction with SiO_2 particles with the formation of hydrogen bonds is sufficient to create mesophases.[115]

The process for the preparation of porous amorphous silica usually includes three stages: synthesis of a gel, drying, and removal of the template. The diameter of pores in MCM-41 can be controlled during the synthesis by varying the type of the reagents used and the conditions of the synthesis. Drying of gels results in only a small shrinkage of pores and has only a small effect on their size, but considerably affects the gel structure. The method and conditions for template removal affect the final size of the pores but not their mutual arrangement. There is still no clear understanding about how the porosity can be controlled at each stage of the preparation of mesoporous SiO_2 (synthesis → drying → template removal) but certain factors determining the porosity have been studied quite thoroughly. For example, the pore size in the SiO_2–surfactant system can be roughly controlled by changing the surfactant 'tail' length. It was found that in the series of surfactants $C_nH_{2n+1}NMe_3Br$, n = 8, 10, 12, 14, 16, 18, the pore size in the resulting product increased by ~0.45 nm (Fig. 9 *a*,*b*) with each increase in n ($\Delta n = 2$). Yet another way to change the pore size is to introduce in the system a non-polar organic solvent [*e.g.*, mesitylene (Fig. 9 *c*,*d*)],[101,116] which is incorporated in the hydrophobic part of micelles during the synthesis, thus increasing their diameter.

The type of the template–matrix interaction affects the thickness of the SiO_2 walls. The silicate mesophases prepared using neutral surfactants have thicker pore walls ($\geqslant$1.7 nm) than the mesophases synthesised on the basis of ionic surfactants (0.8–1.3 nm).[115] There is no strong electrostatic interaction in the case of neutral surfactants; probably, this fact favours the further ordering and provides a product with thicker walls.

The capillary adsorption of gases at their liquid–gas transition temperatures is one of the main methods for the study of mesoporous phases. The results obtained by this method show that the specific surface areas of mesoporous phases are large (~1000 $m^2\ g^{-1}$) and the pore size distribution is narrow (Fig. 10). A detailed study of the gas adsorption in mesoporous matrices[117] showed that the pore size distribution can be calculated from data on the gas partial pressure above a sample (p/p_0) using a modified Kelvin equation:

$$r(p/p_0) = \frac{2V_L}{RT\ln(p/p_0)} + d(p/p_0) + 0.3,$$

where $r(p/p_0)$ is the pore size (nm); V_L is the molar volume of the gas used; γ is the surface tension factor of its liquid phase [$\gamma(N_2) = 8.88 \times 10^{-3}$ N m^{-1}],[117] $d(p/p_0)$ is the thickness of the liquid film adsorbed on the sample (calculated using the Harkins–Jura equation),[117] and 0.3 is the correction for the non-ideality of the system.

Studies of MCM-41 phases by electron microscopy and small-angle X-ray scattering (SAXS) showed that the samples have strictly ordered structures of pores uniformly distributed by size (Figs 9, 11).[118]

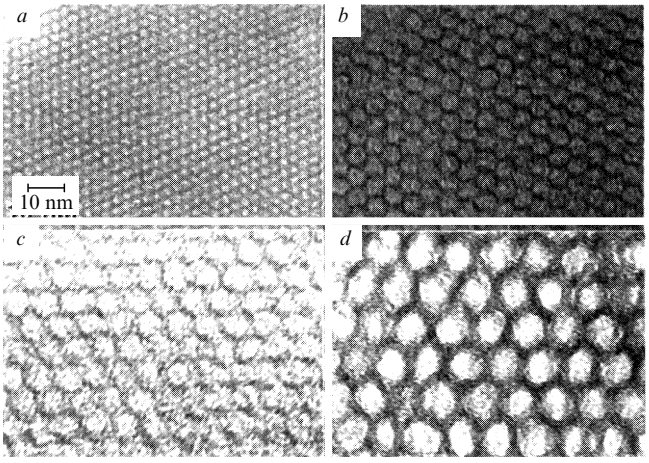


Figure 9. Photomicrographs of MCM-41 samples obtained by TEM.[101] (*a*) $C_8H_{17}NMe_3Br$ template, d = 2 nm; (*b*) $C_{16}H_{33}NMe_3Br$ template, d = 4 nm; (*c*) $C_{16}H_{33}NMe_3Br + Me_3C_6H_3$ template ($C_{16}H_{33}NMe_3Br$: $Me_3C_6H_3$ = 2), d = 6.5 nm; (*d*) same as above ($C_{16}H_{33}NMe_3Br$: $Me_3C_6H_3 > 3$), d = 10 nm.

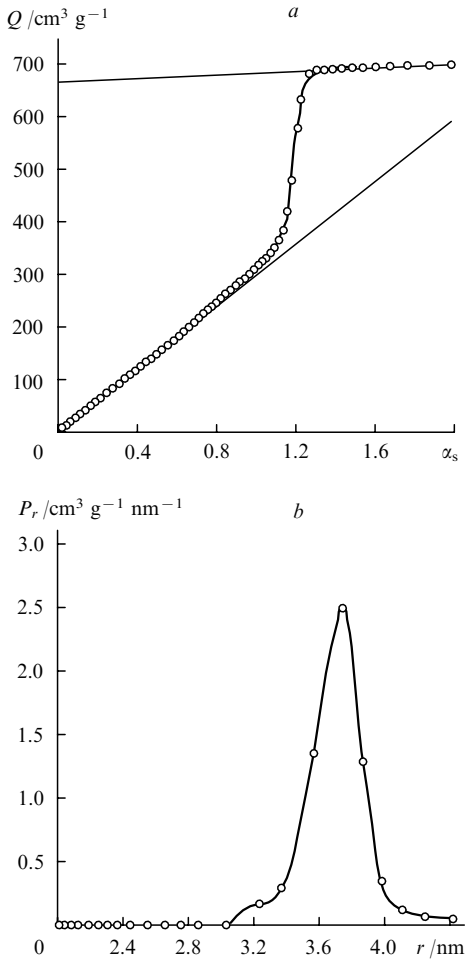


Figure 10. Standard adsorption curve (*a*) and pore size distribution (*b*) typical of MCM-41 molecular sieve.
Notation: α_s is standard adsorption, Q is amount of adsorbed gas, r is pore size, P_r is pore size distribution.

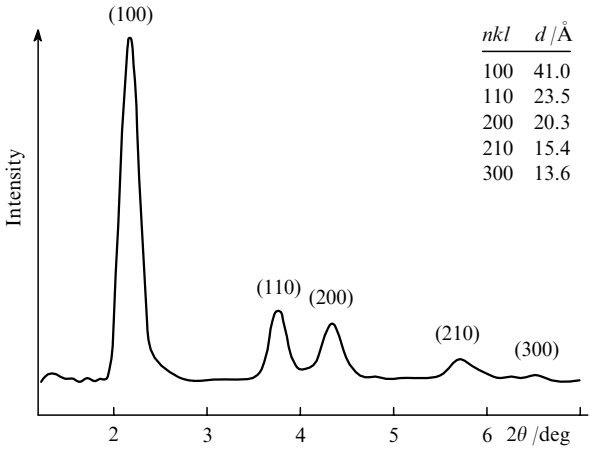


Figure 11. Small-angle X-ray scattering of an MCM-41 matrix.

All these facts make it possible to use materials based on mesoporous silica as catalyst supports, membranes, selective adsorbents, sensor materials and matrices for the preparation of various functional composite materials.

Films of mesoporous silica are of considerable interest since they can be used as media with low dielectric constants in the deposition of multiple-layer integrated circuits. Magnetic nanocomposites based on such films can be used for development of high-density information carriers.

There are various methods for the preparation of mesoporous SiO_2, many of which involve the chemical deposition of films from solutions. Obviously, the formation of mesophases in the synthesis of films occurs similarly to the synthesis of the corresponding bulk samples.

The orientation of films with respect to the plane of the substrate is one of the most important characteristics of films. In the case of mesoporous silica, special attention is paid to the mutual arrangement of the mesopores. As a rule, they are oriented parallel to a substrate, since the film – substrate interaction energy is a maximum for this orientation of micelles. For example, MCM-41 films have the (100)-orientation almost in all cases.‡ Syntheses of oriented films of mesoporous silica on glass, polymeric, graphite, mica and silicon substrates have been described.[119–121]

The ordering of pores in the substrate plane (*i.e.*, the formation of the rolling texture) is much more rare and is only possible if the substrate has a particular direction. The synthesis of epitaxial films of mesoporous SiO_2 on a Si (110) substrate can be

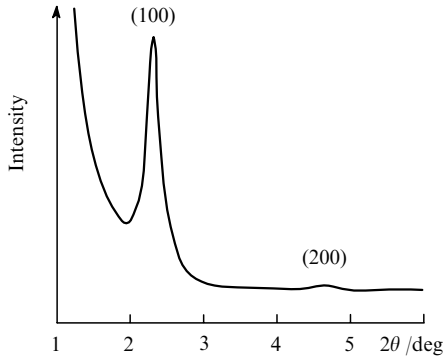


Figure 12. X-Ray diffraction pattern of a mesoporous silica film obtained on a Si (110) matrix.[119]

‡ It should be noted that the films formed at the liquid – gas interface also have the (100)-orientation.

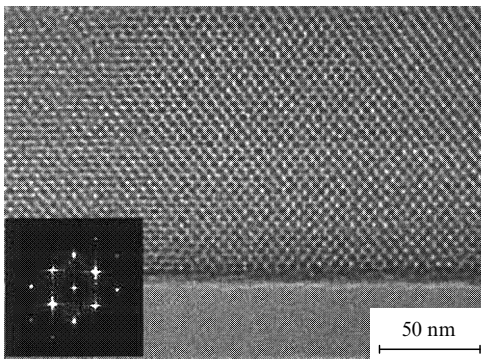


Figure 13. Photomicrograph of the cross section of a mesoporous silica film on a Si (110) matrix (the inset shows electron diffraction data).[119]

mentioned as an example.[119] Figure 12 shows the X-ray diffraction data for such films. The presence of the (100) and (200) diffraction maxima at 2θ values of 2.3° and 4.5° and the absence of the (110) peak suggest that the mesopores are oriented parallel to the substrate. Texture measurements showed that the pores in the substrate plane are oriented parallel to the [100] direction. These results are also confirmed by transmission electron microscopy data for a chip from a sample and by electron diffraction data (Fig. 13). At the same time, the SiO_2 films obtained on Si (100) and Si (111) substrates are not oriented in the substrate plane.

c. The use of mesoporous SiO_2 for the synthesis of nanocomposites

The application range of mesoporous phases and materials based on them is very broad due to their unique properties, such as the large specific surface area, the ordered system of mesopores, the uniform pore size distribution, the high diffusion rate of gases into the material bulk, *etc*. Mesoporous phases find use as catalysts [122] and catalyst supports;[123] matrices for conductive polyaniline [124] and carbon fibres;[125] tiny reactors for redox reactions;[126] selective membranes;[127] adsorbents with large surface area;[101] and porosity standards.[101]

In terms of structural parameters, the nanostructures synthesised inside cylindrical pores are subdivided into bulk nanoparticles, nanowires and nanotubes.[128] The methods for the synthesis of SiO_2-based nanocomposites can be classified into two groups. The first group includes the methods based on the impregnation of a porous material with metal salts followed by the chemical modification of the composite. For example, the synthesis of Ag and Cu nanoparticles in the mesoporous MCM-48 phase grade (mesoporous SiO_2 with cubic structure) was described.[39] MCM-48 samples were impregnated with solutions of $AgNO_3$ and $CuNO_3$ in ethanol and then dried to remove the solvent. During the evaporation of the solvent, the Ag^+, Cu^+ and NO_3^- ions were adsorbed on the silica surface. Reduction of the resulting composites resulted in Ag and Cu nanoparticles (Fig. 14) with sizes (~10 nm) exceeding the pore diameter of mesoporous silica (~3 nm). Presumably, in this case nanoparticles formed outside

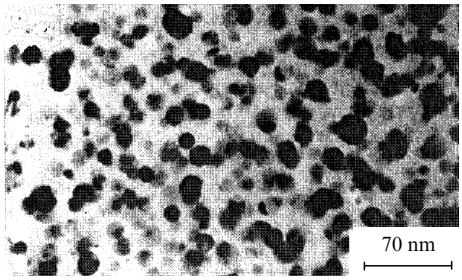


Figure 14. A TEM photomicrograph of mesoporous SiO_2 with incorporated Cu and Ag particles (Ag : Cu = 1 : 3).[39]

the pores. This probably resulted from low hydrophilicity of the inner surfaces of the mesopores [101] that complicated their impregnation with aqueous solutions.[129] As a result, the method for the synthesis of nanocomposites based on the impregnation of mesoporous silica with solutions of metal salts resulted in the formation of large particles.

The second group of methods is based on modifying mesoporous silica with metal complexes (in particular, complexes that form chemical bonds with silicon or oxygen atoms). The complexes can be incorporated in SiO_2 through the gas phase, by impregnation or by electrochemical treatment.

Jinwoo *et al.*[130] described the preparation of filiform Pd particles in the pores of mesoporous silica by incorporation of palladium hexafluoroacetylacetonate through the gas phase into the pores of an MCM-48 or MCM-41 matrix. Before the process, the matrices were annealed for 8 h at 400 °C. The precursor was incorporated into the pores *in vacuo* at 55 °C (as a result, the colour of the sample changed from white to yellow). The subsequent reduction of the palladium complex at 150 °C in a 10% H_2/N_2 mixture gave palladium nanowires (Fig. 15).

Incorporation of siloferrocenophane $[Fe(C_5H_4)_2SiMe_2]$ into the channels of mesoporous silica followed by polymerisation gave iron-containing particles.[128] It should be noted that the polymerisation of siloferrocenophane is accompanied by the formation of a chemical bond between the silicon atom of the complex and the oxygen atoms of mesoporous silica (Fig. 16 *a*), which allows one to decrease the mobility of the complex within the porous structure. Subsequent pyrolysis of the resulting composites in a stream of nitrogen at 900 °C results in the formation of iron monowires in a silica matrix (Fig. 16 *b*,*c*). Unfortunately, the nanoparticles obtained had nonuniform lengths (they filled the pores only partially) and thicknesses (the thickness nonuniformity can be explained by the partial melting of nanocrystalline iron during the annealing).

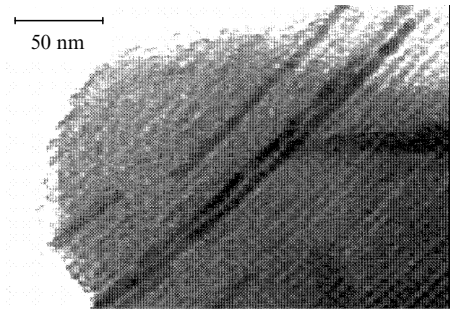


Figure 15. A TEM photomicrograph of Pd nanowires in an MCM-41 matrix.[130]

In the context of the synthesis of uniform particles, the study by Leon *et al.*[129] is of considerable interest. It reports the synthesis of germanium nanoparticles in a mesoporous silica matrix; these particles reproduce the shape and size of the pores. The nanoparticles were obtained by incorporation of Ge_2H_6 into the matrix through the gas phase at a high pressure (5–40 atm) at room temperature followed by thermal decomposition.

The synthesis of nanocomposites by incorporation of a metal complex into a mesoporous matrix in a liquid phase was described by Parala *et al.*[131] The nanoparticles of CdSe were obtained by impregnation of an MCM-41 mesoporous matrix with a solution of Me_2Cd and $(Bu_3P)_2Se$ in tributylphosphine followed by heating to 325 °C in trioctylphosphine oxide. As a result, CdSe nanoparticles with sizes of 3–5 nm formed inside the porous structure of MCM-41.

An alternative method for the synthesis of filiform iron nanoparticles was reported by Napolskii *et al.*[132] A nonpolar iron complex capable of decomposing at low temperatures with weak aggregation of nanoparticles was incorporated into the hydrophobic part of a liquid-crystalline micelle ($C_{16}H_{33}NMe_3Br$) in a mesoporous silica matrix (Fig. 17). $Fe(CO)_5$ was chosen as such a complex. The carbonyl complex was decomposed *in vacuo* under UV irradiation. The particles of metallic iron resulting from the decomposition (Fig. 18 *a*) were shown [133, 134] to contain a considerable fraction of amorphous iron; therefore, it was suggested to additionally crystallise iron particles in the channels of mesoporous silica by annealing in hydrogen flow at moderate temperatures.

The particles obtained after the annealing were characterised by a high anisotropy parameter, which was assessed using two independent methods: the temperature dependence of magnetic susceptibility and the small-angle polarised neutron scattering.[135–137] It was found that decomposition of $Fe(CO)_5$ at high temperatures resulted in a more complete crystallisation of iron, hence the nanocrystals grew lengthwise. Since the diameter of the nanoparticles does not change, this increases the geometrical anisotropy factor. For an iron-containing sample reduced at 375 °C, the anisotropy parameter equals 40, the coercive force is $\sim$450 Œ, and the saturation magnetisation is $\sim$3 emu g^{-1}. Thus, not only nanoparticles were obtained in the pores of mesoporous silica but also their distribution was made homogeneous.

A different approach to the synthesis of nanoparticles in the pores of mesoporous SiO_2 based on the hydrophilisation of the internal surfaces of a silica matrix by ethylenediamine was implemented by Zhang *et al.*[138] The nanoparticles of ZnO (a wide-gap semiconductor) § were obtained by adsorption of Zn^{2+}

§ The interest in ZnO nanoparticles is primarily due to the possibility of employing the latter in elements of short-wave electrooptical devices.

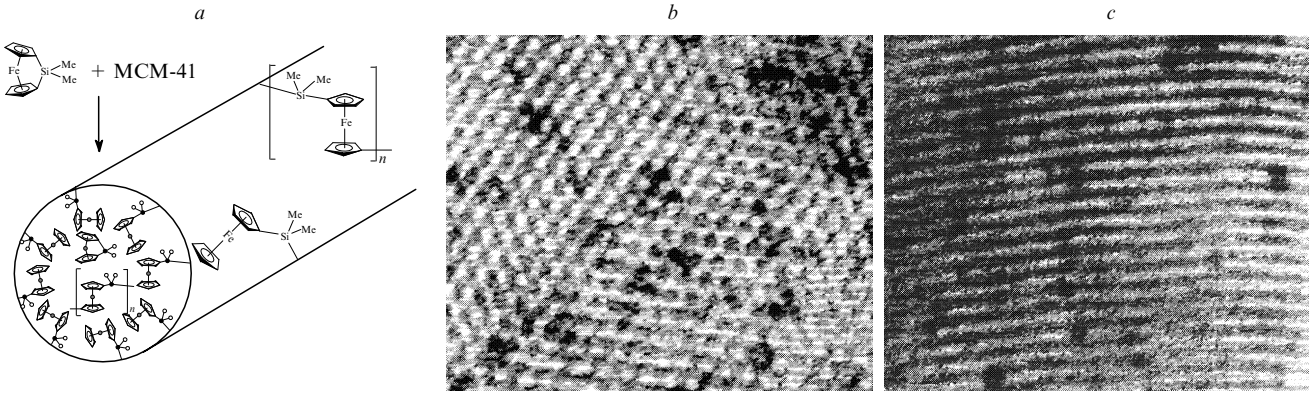


Figure 16. Scheme of the synthesis of iron nanowires in an MCM-41 matrix (*a*) and photomicrographs (*b*, *c*) of the resulting composites (*b* is cross section, *c* is longitudinal section).[128]

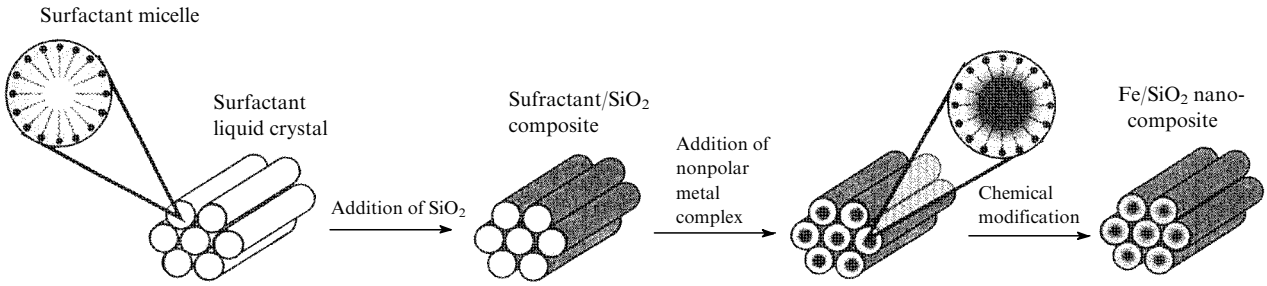


Figure 17. Scheme of synthesising iron nanowires in a mesoporous silica matrix.[132]

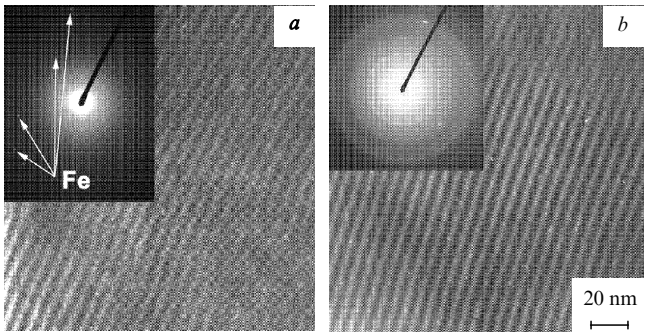


Figure 18. TEM image and electron diffraction (shown in the insets) of iron nanowires in a mesoporous silica matrix obtained by UV irradiation *in vacuo* (*a*) and additional crystallisation at 375 °C (*b*).[133]

cations on a porous silica surface modified with *N*-[3-(trimethoxysilyl)propyl]ethylenediamine followed by annealing in air at 600 °C. In principle, functional groups can be attached to both the internal and external surface of silica. In the latter case, this results in larger ZnO particles on the matrix surface. However, since the major part of the surface of mesoporous silica consists of the internal surfaces of the pores, the reaction of Zn^{2+} cations with ethylenediamine mostly occurs inside the porous structure. TEM data confirm the presence of zinc oxide nanoparticles in the pores of the mesoporous matrix and the absence of large particles on the external surface (Fig. 19). The content of zinc oxide in the samples reaches 9 mass %.

The absorption spectra suggest that the absorption edge of ZnO nanoparticles is shifted to the short-wave region (290 nm), whereas that of macrocrystalline ZnO is at 370 nm (3.1 eV). The considerable blue shift in the absorption spectra is caused by an

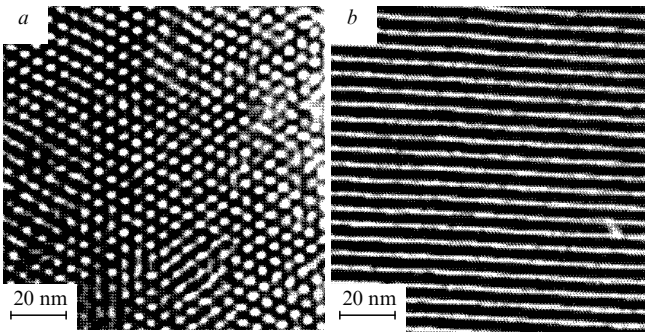


Figure 19. TEM image of ZnO particles in a mesoporous silica matrix;[139] (*a*) cross section, (*b*) longitudinal section.

increase in the band gap, which in turn is a manifestation of the quantum confinement effect. Studies of the photoluminescent properties of zinc oxide nanoparticles show the presence of a rather intense light emission in the blue part of the spectrum ($\sim$460 nm). The suggested method was tried for syntheses of other compounds, but it succeeded only in the case of cobalt oxide. Particles of precious metals such as silver, gold and palladium, as well as particles of nickel and copper oxides, could not be obtained using the method described above.

Particular interest is attracted by the synthesis of one-dimensional nanoparticles utilising films of mesoporous silica, including magnetic nanocomposites for data storage devices with ultra-high density of recording.

The rapid development of information technologies in the past years has necessitated the storage and processing of huge amounts of information, which has required that new devices with ultra-high areal density be created. Principally new magnetic materials with high-precision properties and nonlinear magnetic characteristics have been developed for these purposes.

According to literature data, ferromagnetic nanosized structures are the most promising magnetic materials for storage devices. However, materials based on spherical nanoparticles have low blocking temperatures and a near-zero coercive force at room temperature; therefore, it was suggested to use anisotropic nanoparticles.[139]

Yet another important requirement for magnetic materials based on nanoparticles is that magnetised nanoparticles must be firmly 'fixed' in a matrix to prevent their movement, aggregation and chemical interactions. This can be achieved by synthesising magnetic nanoparticles in nanoreactors. Utilisation of such particles instead of metallic alloys makes it possible to avoid the use of a protective layer on the magnetic data medium and thus to increase the resolution capability of the reading head.

Napolskii *et al.*[132] and Eliseev *et al.*[140] considered the prospects of magnetic nanocomposites obtained on the basis of epitaxial mesoporous SiO_2 films in storage devices with ultrahigh data density. It is known that mesoporous SiO_2 forms epitaxial films on certain supports [*e.g.*, on Si (110)]. It was found that the incorporation of a magnetic material (*e.g.*, iron) into the pores results in an ordered system of magnetic nanoparticles a few nanometres in diameter and several hundred nanometres long (Fig. 20).

Such particles are isolated from each other by silica walls; therefore, exchange interactions between them are sufficiently low.[141] Their geometrical anisotropy is yet another advantage that allows one to stabilise the magnetic moment of a separate particle and increase the coercive force. One more advantage should also be mentioned: the system of magnetic particles in a mesoporous silica reproduces the dimensions, shape and arrangement of pores, hence it is also ordered. This allows a reading head (for example, the tip of a magnetic force microscope) to be positioned with high precision when reading or writing data.[132]

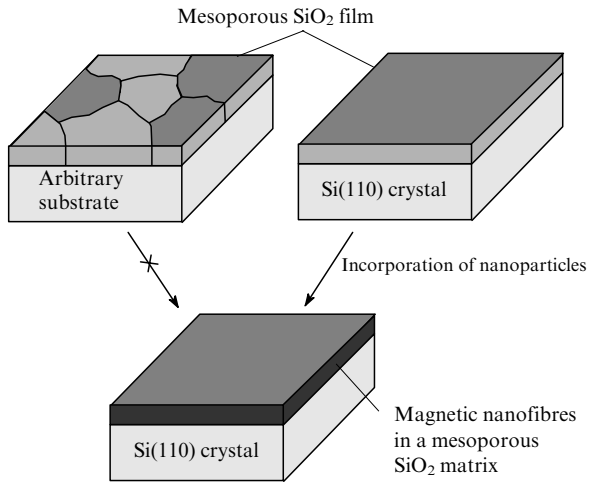


Figure 20. Scheme of growing of epitaxial films of Fe/SiO_2 nanocomposites for devices with ultra-high recording density.

d. Mesoporous aluminosilicates

Mesoporous materials based on silica with an ordered pore arrangement, in which a fraction of silicon atoms are replaced by aluminium atoms, are promising matrices for the synthesis of nanocomposites. Partial replacement of Si atoms by Al atoms in the silica structure creates a negative charge on the matrix, which is proportional to the amount of incorporated aluminium. Cations of transition metals can play the role of positively charged counterions located inside the pores; the number of such ions can be controlled by changing the content of aluminium in the matrix. Reduction of transition metal cations allows one to obtain nanocomposites with a predefined content of a metal phase in the aluminosilicate matrix.

Sasaki *et al.*[142, 143] synthesised platinum nano wires using mesoporous aluminosilicate FSM-16 with a hexagonal arrangement of pores ~ 3 nm in diameter. The matrix was annealed in an oxygen flow at 500 °C, impregnated with an H_2PtCl_6 solution and reduced under UV irradiation in the presence of a propan-2-ol vapour. This gave platinum nanowires 150 – 500 nm long (Fig. 21).

Subsequent utilisation of aluminosilicates for synthesising filiform nanoparticles of transition metals showed [141] that the morphology of nanoparticles in the samples depends on the Si : Al ratio in the aluminosilicate matrices. Nanocomposites containing filiform particles were obtained using aluminosilicate matrices with a small content of aluminium (< 10 mol.%). At higher aluminium concentrations in the matrix, not only nanofibres but also spherical particles with sizes of 3 – 10 nm formed; in this case, the total amount of the transition metal in the nanocomposite decreased. This is presumably explained by the formation of aluminium polyhydroxocomplexes that close the pores and prevent the incorporation of metal ions.

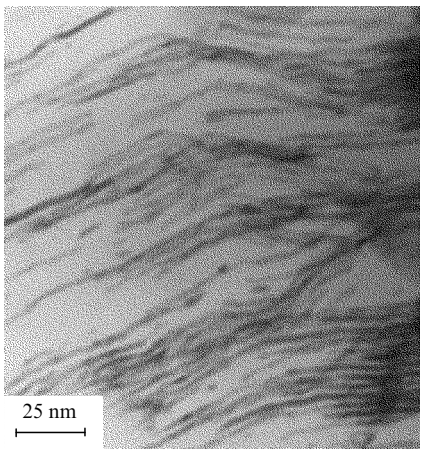


Figure 21. HRTEM photomicrograph of Pt nanowires in an FSM-16 matrix.[143]

Kolesnik *et al.*[144] and Eliseev *et al.*[145] compared the ion-exchanging properties of mesoporous aluminosilicates containing from 5 mol.% to 33 mol.% of aluminium obtained by cohydrolysis of silicon and aluminium compounds or by the hydrothermal method. It was shown that the parameters of ordering of the aluminosilicate structures depend on the hydrolysis rates of silicon and aluminium compounds.[146] It was found that $\sim 90\%$ of the overall number of aluminium atoms present in the reaction mixture are incorporated into the aluminosilicate structure, whereas the remaining 10% form polyhydroxocomplexes and block the pores.

e. Porous alumina

Films of porous alumina obtained by anodic oxidation are intensely studied in the context of their possible utilisation as templates in order to form nanostructured composites. The structures of such films contain an ordered pore system with the closest hexagonal packing, where the pores are arranged at right angles to the substrate surface. Their diameters and distance between the neighbouring pores can be varied in a broad range. The technology for the synthesis of porous alumina and its utilisation as a protective oxide coating has a long history. However, fundamental studies on the processes of self-organisation of nanostructures in a porous alumina matrix started only ten years ago. The latest achievements in the assembly of nanostructures using porous alumina were reviewed by Shingubara.[147] He also considered the utilisation of the resulting nanomaterials as high-density data storage media, functional nanosystems demonstrating quantum confinement effects, high-sensitivity chemical sensors, electronic devices with nanometre sizes and biochemical membranes. The main attention in our review will be given to synthetic approaches to the formation of nanocomposites with ordered structures of active sites in the porous alumina matrix.

The anodic oxidation of aluminium and its alloys in acidic electrolytes have been intensively studied for a long time due to their wide industrial utilisation. An early work [148] describes the structure of the porous alumina cell and the dependence of the lattice cell size on the voltage. A number of publications [149 – 151] report the assumed mechanism of the formation of mesopores during the electrolytic dissolution of aluminium. (Unfortunately, the nature of the nanopore self-organising process has not so far been established unambiguously.) Thompson *et al.*[151] studied the effect of several processes on the formation of nanoporous alumina, including the growth of alumina at the aluminium/alumina interface due to the transfer of Al^{3+}, OH^- and O^{2-} ions from the internal side of the oxide film to the external side, as well as the dissolution and deposition of alumina at the oxide film – solution interface. It is stated [152] that the morphology and conditions for the formation of a hexagonal ordered pore structure in alumina obtained by the anodic oxidation of aluminium in oxalic and sulfuric acids [153] are determined by the dependence of the coefficient of volume expansion of alumina on the anodising voltage and by the oxide formation rate. Nielsch *et al.*[154] assumed that the self-organisation of a structure requires a 10% porosity of the material, irrespective of other anodisation conditions. In other words, it is possible to obtain ordered porous alumina with any size of the lattice cell, provided that the applied voltage and the pH of the electrolyte satisfy the '10% porosity' rule. At present, the difference between the densities of alumina and metallic aluminium is also considered as an important factor for the formation of an ordered porous structure. Since the density of the oxide (~ 3900 kg m^{-3}) exceeds considerably the density of pure alumi-

nium (2698 kg m^{-3}) and electrochemical oxidation occurs only in a thin layer at the oxide film/metal interface, the increase in the density leads to the formation of an ordered porous structure.

The recent outburst of interest in the study of porous alumina was caused by the work by Masuda and Fukuda [155] who described the synthesis of a highly ordered porous alumina structure by two-stage oxidation. Initially, alumina with a highly ordered porous structure at the lower film boundary was obtained by the anodic oxidation of high-purity aluminium for 160 h at 0 °C in 0.3 M oxalic acid at a constant voltage of 40 V. The subsequent selective dissolution of the film in a mixture of 85% H_3PO_4 (35 ml $litre^{-1}$) and CrO_3 (20 g $litre^{-1}$) [156] at 80 °C gave aluminium with highly ordered relief of the surface. The second anodic oxidation of aluminium with such a roughened surface gave an oxide with a highly ordered nanopore structure. Such alumina can be used as a nanoreactor.

Figure 22 shows a typical structure of porous alumina obtained by two-stage anodic oxidation. Scanning electron microscopy data show the hexagonal packing of the nanopores. The mean pore diameter is 36 nm and the distance between the pore centres is ~90 nm. A cross-section of the porous structure (see the inset in Fig. 22) demonstrates the formation of the so-called 'barrier layer' ~30 nm thick with periodic roughness of the aluminium support. The neighbouring pores are separated by side walls ~50 nm thick.

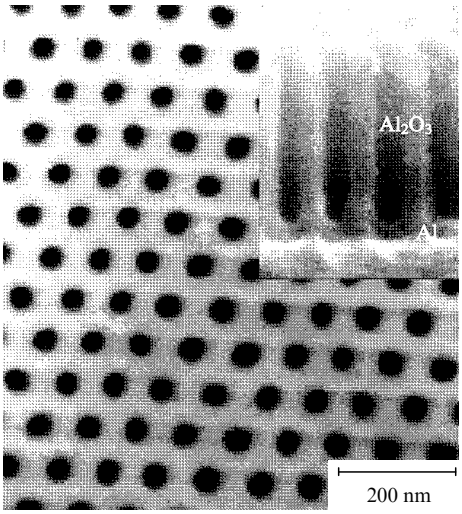


Figure 22. Typical structure of porous alumina obtained by two-stage anodic oxidation. The inset demonstrates the cross section of the film.

The choice of the acid in which the aluminium surface is subjected to anodic oxidation determines the size and geometric arrangement of the nanopores. The anodising voltage (V_a) which provides the formation of a porous alumina with highly ordered pore structure also depends on the acid.

Acid	V_a /V	D_{pore} /nm	D_{cell} /nm
H_2SO_4	25–27	>13	~55
$(COOH)_2$	40	>25	~90
H_3PO_4	195	>200	~500

The dependence of the mean cell size and the diameter of the pores on the voltage of anodic oxidation is shown in Fig. 23 for oxalic acid as the electrolyte.[157] The maximum ordering of the pores is achieved at a voltage of 40 V. The ordering increases with an increase in the duration of the first oxidation and the acid concentration. Masuda *et al.*[158, 159] also studied the conditions of the self-organisation of the porous structure of alumina obtained by the anodic oxidation of aluminium in sulfuric and phosphoric acids.

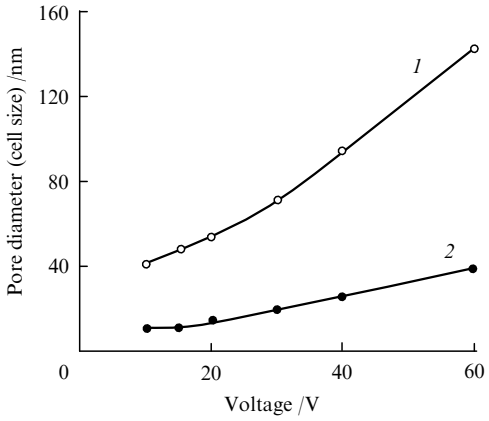


Figure 23. Dependence of the mean cell size (*1*) and pore diameter (*2*) on the anodic oxidation voltage in oxalic acid solution.[157]

Additional etching of the resulting porous material in appropriate acids makes it possible to widen the pores. The cell size of porous alumina differ slightly depending on the electrolyte used (at equal voltages). For example, the cell size in alumina obtained by anodic oxidation at 30–40 V in sulfuric acid is slightly smaller than in that obtained in oxalic acid.

Japanese researchers [160, 161] controlled the formation of mesopores by pretreatment of the starting aluminium surface. To do so, periodic mechanical defects were applied on an aluminium surface (by pressing aluminium with a silicon carbide having a preset surface periodicity at the mesolevel). The press-form was prepared using lithography and dry etching. This approach made it possible to obtain a well-ordered (by depth) pore structure (the ordering zone was 1 mm).

Yet another surface pretreatment method utilises the tip of an atomic force microscope (AFM) to apply defects on aluminium surface.[162] Using a diamond tip, it was found possible to create periodic depressions with a preset depth and geometric arrangement on aluminium surface. This method makes it possible to vary the structure of mesopores in a broad range. In particular, it was used to obtain a thin layer of alumina with a tetragonal pore packing. (As the thickness of the oxide coating increases, the porous structure tends to organise a hexagonal pore packing with a distance of ~90 nm between the pores.) The effect of the distance between the neighbouring defects on the organisation of the porous structure was studied. It was shown that the distance between the neighbouring pores could be varied from 65 to ~100 nm at a constant anodisation voltage of 40 V and that even a small mechanical strain ($\sim 5 \times 10^{-5}$ N) was sufficient for a controlled formation of mesopores by this method.

Alumina with an ordered mesopore structure was used for the synthesis of various nanomaterials. Porous alumina films are used as masks for etching certain materials, as templates for making polymer 'imprints' and as porous matrices for incorporating functional materials by electrochemical, sol–gel and CVD deposition.

Ion or plasma etching of semiconducting materials can serve as examples of the first process. In this case, the porous oxide structure of alumina is copied onto a substrate with a sufficiently high reproducibility.[163–165] Making an 'imprint' of a porous structure on a metal substrate by polymerisation of poly(methyl methacrylate) in the pores of alumina followed by dissolving alumina and sputter-deposition of a metal is a similar process (in this case, porous alumina plays the role of the template).[155] Incorporation of functional components into mesopores of an alumina matrix by electrochemical, sol–gel or CVD deposition is the most popular method for the synthesis of nanocomposites.

Studies of magnetic materials based on porous alumina were started a quarter of a century ago.[166–168] The main purpose of these studies was to create magnetic materials with ultrahigh data

density. The data density on modern data recording media reaches 100 Gb inch^{-2}, and the trend of the growth in the data carrier capacity has been maintained for over four decades. Currently, the possibility of creating materials with data density exceeding 1 Tb inch^{-2} is being studied.

Arrays of densely packed magnetic FePt nanoparticles (Fig. 24) is among the most promising magnetic materials;[169, 170] however, such particles with sizes of about 5–10 nm are in a superparamagnetic state and hence have a zero coercive force at room temperature. Ordered structures could not be obtained from these strongly anisotropic nanoparticles. Free FePt nanoparticles are generally unstable and tend to aggregation, which results in the necessity of creating a protective surface layer; the latter certainly decreases the prospects of using such structures as data media.

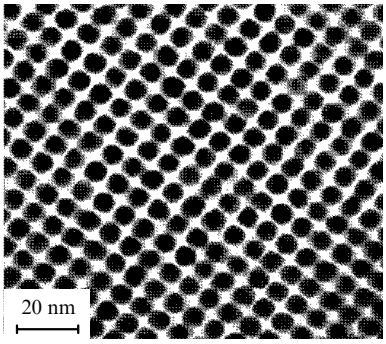


Figure 24. Array of densely packed magnetic FePt nanoparticles.[170]

It could be expected that magnetic nanofibres incorporated in a porous alumina matrix would satisfy the requirements for state-of-the-art data media. The simplicity of creating structures with high geometric anisotropy in the direction perpendicular to the substrate plane makes porous alumina very promising for the development of magnetic materials. Numerous publications are known that deal with the synthesis and study of nanoparticles of nickel,[171–176] iron,[172, 175, 177, 178] cobalt,[172, 175, 179–181] platinides,[173] lead [178] and alloys such as CoFe [182] and NiCo.[183]

Pulse deposition and electrodeposition with alternate current are the most efficient methods to synthesise metals in a porous alumina (deposition with direct current is accompanied by breakdown of the double electric layer, which results in the formation of large particles on the alumina surface). The use of electrodeposition of functional materials into alumina pores encounter a serious problem due to the existence of an Al_2O_3 barrier layer between the aluminium substrate and the lower boundary of a pore. Therefore, various methods have been developed for the removal of the barrier layer.[171, 184] The method for decreasing the barrier layer thickness by gradually decreasing the anodic potential [166] is recognised as the most successful. Yet another problem is that the formation of nanoparticles occurs at the porous structure–substrate interface and diffusion of solution ions to this interface is hindered; because of this, an important role in electrodeposition belongs to the time between successive deposition pulses.[171]

Magnetic Co nanowires with diameters of 10 to 60 nm and with distances of 60 to 120 nm between the adjacent wires (Fig. 25 *a*) were obtained using a porous alumina matrix synthesised by the anodic oxidation in oxalic or sulfuric acid. An HRTEM study of the cross-section of an array of nanofibres showed that the fibres consisted of partially aggregated cobalt nanoparticles (Fig. 25 *b*).[79]

An important advantage of the alumina matrix as a nanoreactor is that it is possible to obtain ferromagnetic fibres of different lengths by varying the duration of electrodeposition. Figure 26 shows the magnetic reversal curves for Co nanowires 5,

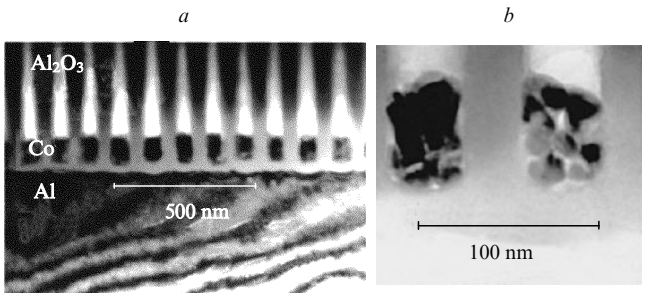


Figure 25. Cross section of an array of magnetic cobalt particles in a porous alumina matrix (*a* and *b* designate different magnifications).[79]

60 and 220 nm long. There are apparent differences in the magnetic anisotropy of such nanowires: cobalt nanowires ~5 nm long have a preferential anisotropy in the substrate plane, whereas longer wires (220 nm) are characterised by anisotropy in the direction perpendicular to the substrate. Thus, the magnetic anisotropy of ferromagnetic wires is mainly determined by the shape of the particles; this behaviour is typical of all ferromagnetic compounds. For iron fibres, there is a critical diameter corresponding to the maximum coercive force (2640 Œ) at room temperature [177] (at 5 K, no maximum on the 'coercive force–fibre diameter' plot was found).

In the $Fe_{1-x}Co_x$ system ($0 < x < 1$) obtained by controlled electrodeposition of the components,[182] a transition from the *bcc* crystal structure (Co content ~33%) to a mixed *hcp–fcc* structure (cobalt content ~67%) was observed. However, the coercive force was found to be almost the same for nanowires of both compositions and 9 nm in diameter: ~2900 Œ (for $Fe_{0.67}Co_{0.33}$) and ~2850 Œ (for $Fe_{0.33}Co_{0.67}$). Thus, the size and anisotropy of nanoparticles are the main factors determining the magnetic characteristics of ferromagnetic particles in the nanometre region.

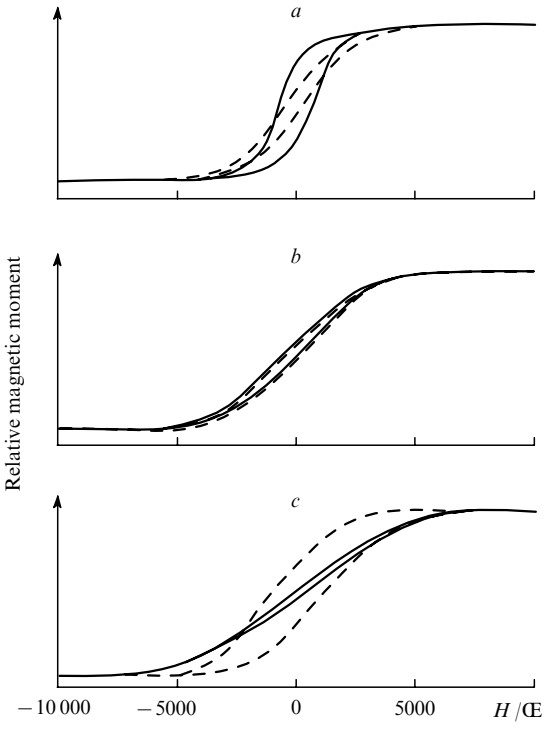


Figure 26. Magnetisation reversal curves for cobalt nanowires 5 nm (*a*), 60 nm (*b*) and 220 nm long (*c*) in a porous alumina matrix (solid line: the field is directed at right angle to the matrix plane; dashed line: the field is directed parallel to the matrix plane).

At the same time, decrease in the nanofibre diameter to 9 nm does not result in superparamagnetism. Calculations show that achieving a data density of about 1 Tb inch^{-2} requires that the distance between the adjacent nanofibres does not exceed 25 nm. This density has not been achieved to date.

In addition, optical nanostructured materials based on porous alumina arouse much interest because they possess a high luminescence intensity. Although the pore sizes in mesoporous alumina exceed the characteristic size required for the quantum confinement effect, it still has good luminescent properties that are not typical of bulk materials. First, porous alumina itself has luminescence in the blue region of the spectrum with a maximum intensity at 460 nm.[185] This emission band appears due to the formation of ionised oxygen vacancies (F^+-centres) in the strongly defective porous structure. The emission intensity can be further intensified by annealing the film at elevated temperatures.

High emission intensities were observed when the structure of mesoporous alumina was filled with zinc oxide. ZnO nanoparticles were synthesised in the matrix by hydrolysis of $Zn(OBu)_2$ in an aqueous medium.[186] The maximum luminescence intensity (485 nm) of zinc oxide nanoparticles approximately coincides with the maximum of irradiation from pure nanostructured ZnO, but the emission intensity of ZnO nanoparticles incorporated in a porous alumina matrix is almost 20 times higher, probably due to the increase in the number of ionised oxygen vacancies in ZnO nanoparticles located inside the alumina pores.

Several publications are available on the synthesis of optically active CdS nanowires prepared by electrodeposition;[187] and Bi_2Te_3;[188] titania doped with terbium or erbium (the sol–gel method);[189, 190] GaN nanoparticles (the sol–gel method),[164, 191] as well as dyes such as Rhodamine 6G and aluminium 8-hydroxyquinolinate[192] in a porous alumina matrix. It was suggested[184] to use anodised alumina for making electroluminescent materials; the aluminium substrate served as the cathode and a layer of conductive glass (ITO) served as the anode (the optically active component was incorporated into the pores). All these studies show the prospects of utilising nanostructures based on porous alumina films as electroluminescent materials.

Yet another use of porous alumina is related to the synthesis of two-dimensional photonic crystals. It is well known that photon band gap appears only if there is a highly ordered porous structure in sufficiently large areas. For this reason, the technology of aluminium pretexturing followed by anodic oxidation was developing in recent years.[157, 160, 161] This approach made it possible to obtain two-dimensional photonic crystals with a photon band gap in the visible spectral region.[193–197]

Porous alumina can be used to create field emitters based on carbon nanotubes. To do so, nanoparticles of metallic cobalt are electrochemically deposited in the pores of alumina (cobalt particles commonly used as catalysts for growth of carbon and carbon nitride nanotubes).[198–205] A photomicrograph of such an emitter is shown in Fig. 27.

Films of porous alumina are also promising as membrane materials. The transport of lithium ions[206] and other one-, two-[207] and trivalent cations[208] depends on the pore diameter, the pH of the medium and the ionic strength of the solution, as well as on the hydraulic permeability[209] of membranes. It is well known that the conductance of porous alumina considerably depends on the humidity. In view of this, an attempt was made to use a cell consisting of a layer of porous alumina compressed between metallic electrodes as a humidity sensor.[210] It was found that in the range from 50 to 100 ppm^{-1}, there is an almost linear dependence of the capacitance of this element on the air humidity, *i.e.*, such sensors are highly sensitive to humidity.

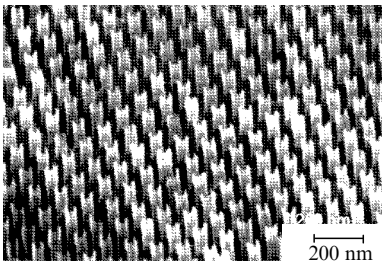


Figure 27. A scanning photomicrograph of a field emitter based on nanotubes synthesised in the pores of alumina.

It follows from the examples considered above that porous alumina is very a promising material for creating nanomaterials for magnetic data storage media, electronic devices, sensors and biomembranes. At present, methods for the synthesis of porous alumina with a pore diameter of $\leqslant 5$ nm are being developed in order to study quantum confinement effects, along with methods for the synthesis of porous membranes on solid semiconducting substrates characterised by high mechanical stability.

3. Synthesis of nanoparticles in two-dimensional nanoreactors. Layered double hydroxides

For two-dimensional nanoreactors, it is most efficient to use layered structures with variable dimensions of the structural cavities. The layers in such compounds are bound by weak van der Waals forces, hence the interlayer distance can be varied easily. Moreover, a layered structure allows one to accelerate considerably the diffusion of gases in the interlayer space and thus facilitate the chemical modification of layered compounds.[211, 212]

Several dozens of studies on the synthesis of nanocomposites using layered matrices have been published (see, *e.g.*, Refs 213–219). The compounds with negatively charged layers and cations in the interlayer space, *viz.*, aluminosilicates, are utilised the most widely. However, such compounds are generally nonstoichiometric, strongly hydrated and have cross-links between the layers; this complicates considerably the synthesis of nanomaterials on their basis and adversely affects the reproducibility of the results.[220, 221] This certainly prevents systematic studies on the mechanisms of nanostructure formation in layered matrices.

Layered double hydroxides (LDHs) with the composition $M^{2+}_{1-x}M^{3+}_x(OH)_2[X^{n-}_{x/n}\cdot m\,H_2O]$ (X is an anion) are the most widespread two-dimensional nanoreactors.[222] To date, compounds with $M^{2+} = Mg^{2+}$, Zn^{2+}, Fe^{2+}, Co^{2+}, Ni^{2+}, Cu^{2+}, Cd^{2+}, Sn^{2+}, Mn^{2+}, Pd^{2+}, Pt^{2+} and $M^{3+} = Al^{3+}$, Fe^{3+}, Cr^{3+}, Mn^{3+}, Ga^{3+}, In^{3+}, Bi^{3+}, Y^{3+}, La^{3+}, V^{3+}, Rh^{3+}, Ir^{3+} and Ru^{3+} have been obtained (see Refs 223–230). As a rule, the radii of the M^{2+} and M^{3+} cations participating in the formation of a layered structure should not differ more than 1.5-fold.[231] Virtually any anion or anionic complex can serve as the X^{n-} anion.[232] The structure of an LDH is a system of positively charged hydroxide layers $[M^{2+}_{1-x}M^{3+}_x(OH)_2]^{x+}$ and anions located in the interlayer space (Fig. 28).[233, 234] In addition to anions, the interlayer space commonly contains labile water molecules.[235] The LDH structure as a whole is stable due to the electrostatic interaction between the positively charged hydroxide layers and the interlayer anions bearing negative charges.

LDHs with the compositions $Li_{1-x}M^{3+}_x(OH)_2.[X^{n-}_{(2x-1)/n}\cdot m\,H_2O]$ $(x > 0.5)$[236] and $M^{2+}_{1-x}M^{4+}_x(OH)_2.[X^{n-}_{2x/n}\cdot m\,H_2O]$, where $M^{4+} = Zr^{4+}$, Ti^{4+}, Sn^{4+} or Se^{4+}, are also known (see Refs 237, 238). Moreover, cation-substituted layered hydroxides have been synthesised that contain several cations in oxidation states 2+ and/or 3+, *e.g.*, $M^{2+}_{1-x-y}(M')^{2+}_yM^{3+}_x(OH)_2[X^{n-}_{x/n}\cdot m\,H_2O]$ or $M^{2+}_{1-x-y}M^{3+}_x(M')^{3+}_y.(OH)_2[X^{n-}_{(x+y)/n}\cdot m\,H_2O]$.[239–241]

The vast majority of LDHs crystallise in the trigonal (rhombohedral) system. Hydrotalcite, a natural mineral with the composition $Mg_6Al_2(OH)_{16}[CO_3\cdot 4\,H_2O]$, has this structure. Compounds with the general formula $Mg_{1-x}Al_x(OH)_2[X^{n-}_{x/n}\cdot m\,H_2O]$ and with rhombohedral unit cells are called hydrotalcite-like compounds. Samples with the hydro-

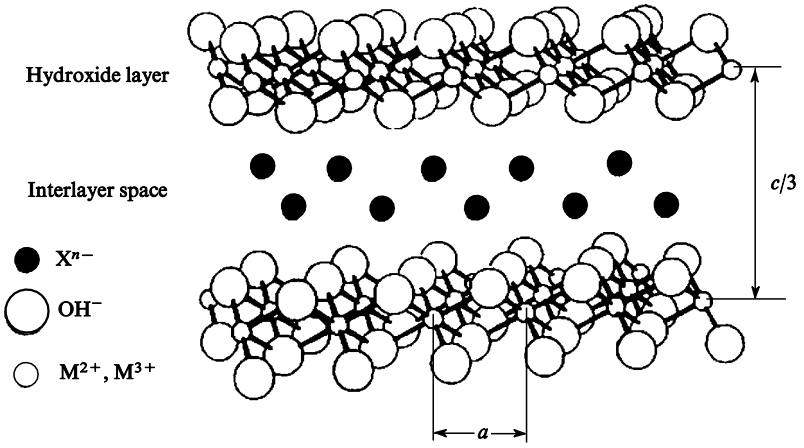


Figure 28. Structure of layered double hydroxides.

talcite structure and with x from 0.05 to 0.4 and m from 0 to 2 were obtained under laboratory conditions.

It should be noted that the arrangement of anions in the interlayer space can vary.[232, 242, 243] For example, the synthesis of LDHs with intercalated polyoxometallates, which have cylindrical symmetry, can result in two types of structures, *viz*., those with parallel and perpendicular arrangement of anions with respect to the hydroxide layers.[244] As a rule, anions are located in the interlayer space in such a way that its dimensions are minimised. However, as the $M^{3+}:M^{2+}$ ratio increases, the positive charge of the hydroxide layers also increases and more anions are required to compensate for it. If the charge of the anions is small, they can fail to fit in the interlayer space due to steric hindrance. Therefore, as the concentration of anions in the interlayer space increases, they need to be grouped into structures that are packed more densely. This is achieved either by arrangement of cylindrical anions at right angles to the hydroxide layers or by arrangement of anions in the interlayer space in two layers parallel to the hydroxide layers; in any case, this results in an increase in the interlayer distance. As a rule, if the unit cell parameter c and the anion size are known, it is possible to determine exactly which type of structure will be realised in a specific case.[245]

Layered double hydroxides have a number of unique properties that are important for the directed synthesis of nanomaterials. The stability of the layered structure of LDHs in a wide range of cation and anion sizes is among these properties. For example, samples of Mg-Al-LDHs containing various anions with sizes from 0.3 to 5 nm in the interlayer distance have been obtained. Furthermore, the number of anions present in the interlayer space of an LDH is determined by the $M^{z+}:M^{3+}$ ratio, which is easy to control during the synthesis. This makes it possible to obtain LDHs with preset stoichiometric compositions and hence to vary the concentration of reaction centres in a matrix.

The thermal stability of LDHs is yet another important property (thermal decomposition of LDHs occurs with retention of their layered structure). As a result, chemical reactions involving anions located in the interlayer space (*e.g*., reduction with hydrogen required for the preparation of magnetic nanocomposites) can be performed at elevated temperatures almost without destruction of the matrix that confines the reaction zone.

These properties open up rich possibilities for the chemical design of nanocomposite materials based on LDHs. First, the wide choice of cations makes it possible to choose a matrix that would satisfy the entire set of properties required from a material. For example, a diamagnetic matrix can be chosen for the synthesis of magnetic nanomaterials, or a matrix that is optically transparent in a specific spectral region can be selected for the preparation of optical nanocomposites. Second, by varying the $M^{2+}:M^{3+}$ cation ratio (*i.e*., the x value) and selecting a particular anionic complex and a chemical modification method, it is possible to vary widely the size and shape of nanoparticles.

Coprecipitation of hydroxides of M^{2+} and M^{3+} metals with an alkali from solutions of their salts at a controlled pH is the main method for synthesising LDHs.[246] To obtain an LDH with desired anions in the interlayer space, the coprecipitation is carried out in the presence of these anions in the initial solution:

$$(1-x)\,M^{2+} + x\,M^{3+} + 2\,OH^- + (x/n)\,X^{n-} \longrightarrow$$
$$\longrightarrow M^{2+}_{1-x}M^{3+}_{x}(OH)_2[X^{n-}_{x/n}].$$

It should be taken into account that if two or more types of anions are present in the solution, one of them will be incorporated preferentially.[247] The ability of anions to undergo preferential incorporation into the interlayer space is often called the selective intercalation constant of an anion. It depends both on the nature of the LDHs and on the conditions of the synthesis (pH, temperature).

A number of techniques are used to obtain LDHs with different anions in the interlayer space. LDHs in the carbonate or chloride form are usually utilised as the starting compounds.

Coprecipitation in the presence of an anion (the method described above). This method is very easy to implement but it does not allow one to obtain LDHs containing just one type of anions in the interlayer space. For this reason, it is only used where the required anion has a high selective intercalation constant.

Direct exchange of anions. This method is based on the anion-exchange properties of LDH.[248] If hydrotalcite (the carbonate form of LDH) is placed in a solution containing the required anion X^{n-}, partial exchange of carbonate ions for X^{n-} occurs, *i.e*., intercalation of the required anion into the interlayer space:

$$Mg_{1-x}Al_x\,(OH)_2[(CO^{2-}_3)_{x/2}] + (x/n)\,X^{n-} \rightleftharpoons$$
$$\rightleftharpoons Mg_{1-x}Al_x(OH)_2[X^{n-}_{x/n}] + (x/2)\,CO^{2-}_3.$$

Since the CO^{2-}_3 anions have a high selective intercalation constant, their complete displacement requires that hydrotalcite be repeatedly treated with a solution of X^{n-} (see Ref. 249). The main advantages of the ion-exchange method include its simplicity and the possibility of obtaining practically pure anion-substituted LDHs. However, the use of the ion exchange method does not allow one to obtain LDHs with large anions that generally have low selective intercalation constants. According to Drezdzon,[250] anion exchange is practically impossible if the size of X^{n-} exceeds 0.6–0.7 nm.

Syntheses of LDHs containing large anionic complexes by anion exchange usually involve sonication. For example, the synthesis of Mg-Al- and Zn-Al-LDHs containing anionic complexes of heteropolymetallates with sizes up to 1.5 nm by

exchange of NO_3^- anions for the corresponding anionic complexes on ultrasonic treatment of the system was described.[251,252]

Interaction of an X^{n-} solution with layered double oxides (LDOs). The method is based on the so-called 'memory effect' that is shown by LDOs obtained by thermal decomposition of LDHs. This effect was found by Chibwe and Jones[253] who showed that treatment of Mg-Al-LDOs with a dilute solution of a salt results in their rehydration to give LDHs with solution anions intercalated into the interlayer space:[254]

$$Mg_{1-x}Al_x(OH)_2[(CO_3)_{x/2}] \xrightarrow{150\ ^\circ C} \longrightarrow Mg_{1-x}Al_xO_{1+x/2} + H_2O + (x/2)\,CO_2,$$

$$Mg_{1-x}Al_xO_{1+x/2} + (x/n)\,X^{n-} + (1+x/2)\,H_2O \longrightarrow Mg_{1-x}Al_x(OH)_2[X^{n-}_{x/n}] + x\,OH^-.$$

Melt technique is based on the intercalation of carboxylate anions into LDHs. This method was implemented by heating a mixture of a solid carboxylic acid and hydrotalcite (or the corresponding LDO) at a rate of no more than 10 deg min^{-1} to a temperature $\sim$10 °C higher than the melting point of the acid.[255] The mixture was kept for 8 h at this temperature and then cooled to room temperature at a rate of $\sim$10 deg min^{-1}.

Many functional properties of materials based on LDHs are related to the special properties of anions intercalated into them. For example, the high reactivity of catalysts based on LDHs is usually due to the catalytic properties of the intercalated ions or products of their thermal decomposition. Depending on the nature of the anion, LDHs can show various magnetic, optical and electrophysical properties. For example, the presence of polymeric anions in the interlayer space induces unusual viscoelastic properties.[248,256]

Due to the sufficiently high interlayer distance in LDHs, diffusion of gases into the interlayer space occurs rather fast. This property is very important for the creation of catalysts and sensor materials with short response times. Moreover, the large interlayer distance makes it possible to perform the chemical modification of LDHs with various gaseous reagents without damaging the layered structure.

Layered double hydroxides are widely employed as catalysts for various organic reactions. Hydrotalcite-like LDHs with intercalated ions of polyoxometallates and Ni-containing LDHs obtained by thermal decomposition or reduction of various nickelates to metallic nickel by treatment with hydrogen are used most widely.[257–259]

Tichit *et al.*[260] describes a hydrogenation catalyst obtained by reduction of $Ni_{2.82}Al(OH)_{7.64}[(NO_3)_{0.17}(CO_3)_{0.41}\cdot 2.46\,H_2O]$ with hydrogen (T = 700 °C). It is a composite consisting of particles of metallic nickel and Al_2O_3; the sizes of these particles are several hundred nanometres. This catalyst is currently among the best nickel-based hydrogenation catalysts.[261]

There are several reasons that explain the popularity of LDH-based catalysts. First, owing to the high specific surface area and the presence of a rather wide interlayer space, they show a high catalytic activity. Second, a hydroxide matrix is an inert carrier for polyoxometallates that does not impair their catalytic properties over the entire lifetime of the catalysts. Third, both hydrotalcite-like LDH-catalysts in the polyoxometallate form and Ni-containing LDH-catalysts can operate at temperatures up to 800 °C without losing their catalytic properties and without a considerable decrease in the specific surface. Finally, the bulk distribution of the catalytic sites (polyoxometallates or metallic nickel) in such catalysts is very homogeneous, which increases the relative catalytic activity per unit mass. Moreover, the preparation of LDH-based catalysts is not too difficult. In fact, LDH-catalysts with polyoxometallate ions intercalated into them became strong competitors for classic oxide catalysts (SiO_2, Al_2O_3) impregnated with salts of various polyoxometallates.[262–264]

Some LDHs find use as solid electrolytes and electrodes due to the ionic conductance they possess.[265–268] The rather high ionic conductance of LDHs results from the high mobility of anions in the interlayer space. For example, the conductance of $Zn_2Cr(OH)_6[Cl\cdot m\,H_2O]$ at 17 °C is $10^{-3}\ \Omega^{-1}\ cm^{-1}$. Replacement of chloride ions by other anions decreases the conductance of this LDH to $10^{-4}\ \Omega^{-1}\ cm^{-1}$ (see Ref. 269). The authors called such compounds 'quasi-two-dimensional' electrolytes due to their high ionic conductance and layered structure. The ionic conductance of LDHs enables their practical application in sensors.[270,271]

The existence of rigid hydroxide layers that confine the interlayer space in the LDH structure creates conditions for the synthesis of nanosystems similar to conditions for their synthesis in nanoreactors.

The possibility of synthesising nanostructures with the use of LDHs was studied by a number of scientific groups. For example, the synthesis of a composite of cadmium sulfide nanoparticles and a solid solution of cadmium and zinc sulfides in the interlayer space of LDHs was reported.[272] An Mg-Al-LDH with intercalated $Cd(edta)^{2-}$ complex was used as the starting compound. The latter was obtained by treatment of an Mg-Al-LDO with an aqueous solution containing the above complex. Unfortunately, the EDTA-complex of cadmium used in this study was contaminated with nitrate ions that were also intercalated into the interlayer space. As a result, a compound with the composition $Mg_{0.654}Al_{0.346}(OH)_2[\{Cd(edta)\}_{0.075}(NO_3)_{0.196}\cdot 1.13\,H_2O]$ was obtained.

The size of the interlayer space in this compound was 0.285 nm (X-ray diffraction data). Since this distance matched the size of the Cd complex in the planar four-coordinate state (0.280 nm), it was assumed that the $Cd(edta)^{2-}$ complex was arranged in the interlayer space parallel to the hydroxide layers. The substituted LDH was sulfidised with sodium sulfide. The formation of cadmium sulfide follows from the change in the LDH colour from white to yellow and the appearance of cadmium sulfide reflections in the X-ray diffraction diagram. In fact, according to X-ray data, the interlayer distance in the LDH virtually did not change during the sulfidising, while the reflections of cadmium sulfide broadened considerably. Presumably, the sulfide was formed in the interlayer space of the LDH as plates no thicker than the interlayer distance (0.285 nm). However, this conclusion disagrees with spectrophotometric analysis data, according to which the absorption band edge for the samples obtained lies in the region of 460–480 nm; these values correspond to particles larger than 10 nm. This fact probably suggests that cadmium sulfide is most likely formed not only in the interlayer space but also on the surfaces of LDH particles. This conclusion is supported by the fact that sulfidising inevitably involves the anion exchange of interplanar ions for sulfide ions from the solution. In this case, sulfidising of the deintercalated cadmium complex should occur directly on the surfaces of the LDH particles.

Sato *et al.*[213,219,273–275] obtained nanosized cadmium and zinc sulfides using other layered compounds such as montmorillonite $\{(Na,K,Ca)(Al,Fe,Mg)[(Si,Al)_4O_{10}](OH)_2\cdot n\,H_2O\}$, $H_4Nb_6O_{17}$ and $H_2Ti_4O_9$.

Isupov *et al.*[276–281] studied the thermolysis of Li-Al-LDHs containing EDTA-complexes of certain transition metals. They showed that the thermal decomposition of $LiAl_2(OH)_6[\{M(edta)\}_{0.5}\cdot 2\,H_2O]$ (M = Cu, Co, Ni) *in vacuo* in an Li-Al oxide matrix resulted in nanoparticles of the transition metal M and that the size and morphology of the nanoparticles depended on the metal selected and on the decomposition conditions.

Thermolysis of Cu-containing LDHs at 400 °C gives spherical copper particles with sizes of 2–5 nm (in the interlayer space of the matrix) and 5–80 nm (on the surface), whereas thermolysis of Ni-containing LDHs gives spherical nickel particles with a $\sim$5 nm diameter and a very narrow size distribution. An increase

in the thermolysis temperature to 800 °C results in a growth in the particle size to 15 nm with a simultaneous broadening of the distribution. At the same time, thermolysis of Co-containing LDHs at 400–800 °C results in large (~100 nm) metal particles in the shape of disks, the size and morphology of which is virtually independent of the thermolysis temperature. It was shown that the reduction of the metal in the complex starts almost simultaneously with the end of the dehydration of the layered matrix. The formation of nanosized particles was explained by the influence of the matrix on the reduction process. Unfortunately, no conclusions were made concerning the reasons for the changes in the dependence of the size and morphology of the nanoparticles on the metal chosen and on the thermolysis conditions. It should be noted that decomposition of LDHs is accompanied by pyrolysis of the organic ligand to give amorphous carbon; as a result, final product is considerably contaminated with admixtures of metal carbides and the material loses its functional properties.

The formation of LDHs and the synthesis of nanocomposites on their basis were also studied by Tretyakov *et al.*[66, 282–292]

They performed[286, 291, 292] a detailed study of the anisotropy of iron and nickel nanoparticles obtained by reduction of anion-substituted Mg-Al-LDHs with different compositions in a stream of hydrogen at different temperatures (300–1000 °C). Based on electron microscopy data and magnetic measurements, the concentration dependences of the transverse and longitudinal anisotropy of metal nanophase reduced at different temperatures (see Ref. 66) were plotted. It was shown that, depending on the composition of the starting anion-substituted LDHs, metal nanoparticles with different dimensionality, *viz.*, from one- to three-dimensional, were formed in this system. An increase in the content of the metal complex in the LDH matrix resulted in a decrease in the dimensionality of the nanoparticles that formed and an increase in the anisotropy factor. It should be noted that the reduction temperature almost did not affect the morphology of the nanoparticles formed: an increase in the reduction temperature increased only the mean size of the nanoparticles, whereas their anisotropy changed insignificantly.

Yet another direction of studies by this group of researchers involved the synthesis of semiconducting nanostructures in the MS/Mg–Al–O system (M = Pb, Zn, Cd).[289, 290, 293, 294] They showed that direct sulfidising of Pb, Zn and Cd complexes intercalated in LDH in a stream of hydrogen sulfide at room temperature is unsuitable for the synthesis of MS/LDH nanocomposites. Therefore, they suggested using LDH systems where the formation of sulfides resulted from the decomposition of an intercalated sulfur-containing metal complex. Thiosulfate, thiocyanate and diethyldithiocarbamate compounds of Pb, Zn and Cd were used as such complexes. Decomposition of the latter ($T_{decomp} < 200$ °C)¶ in the interlayer space occurred without degradation of the LDH structure. For example, PbS/LDHs were obtained by thermal (100–200 °C) or photochemical (UV irradiation at 77 K) decomposition of $Mg_3Al(OH)_8 \cdot [\{Pb(S_2O_3)_2\}_{0.5} \cdot m\,H_2O]$.[290]

A considerable amount of attention was paid to the optical properties of the products obtained. High-resolution spectroscopy in the visible and UV spectral regions showed that the absorption edge for the PbS/LDH samples obtained by thermal treatment was within 500–750 nm. An increase in the annealing temperature shifts the absorption edge to the long-wave region, which indicates an increase in the particle size. Calculations show that the particle size changes insignificantly and lies within 3–5 nm for all the samples obtained. The spectrum of the sample obtained by UV irradiation shows additional maxima at ~580, ~400 and ~300 nm (Fig. 29) [for comparison, Fig. 29 also shows the spectra for the sample obtained by thermal decomposition (dashed line)]. These values are in good agreement with the $1S_e-1S_h$, $1S_e-1P_h$ and $1S_h-1P_e$ exciton transitions of lead sulfide.

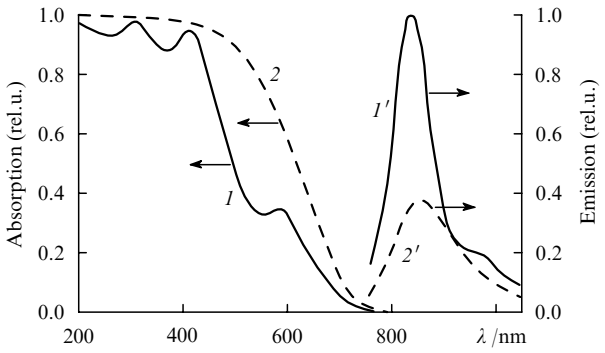


Figure 29. Absorption (*1*, *2*) and photoluminescence spectra (*1′*, *2′*) of PbS/LDH nanocomposites obtained by thermal decomposition at 200 °C (dashed line) and by decomposition under UV irradiation (solid line).[290]

These transitions are usually not observed in the spectra of PbS but they appear in the spectra of the PbS sol synthesised in the presence of polyvinyl alcohol.[295] Similar spectra were also obtained for nanoparticles of lead sulfide stabilised by protein molecules.[296] It is believed that the appearance of forbidden exciton transitions in PbS spectra is due to the modification of the nanoparticles' surfaces.

The photoluminescence spectra of the samples obtained by annealing at 200 °C and by UV photolysis are shown in the right part of Fig. 29. Each spectrum is characterised by the presence of two peaks at λ = 840 and 910–940 nm: the first one corresponds to the luminescent transition over the band gap, whereas the second one corresponds to the transition over the energy levels formed by surface defects. It should be noted that the integral intensity of the luminescence peak of the main state (transition over the band gap) for the sample obtained by UV irradiation is about four times higher than that for the sample obtained by annealing at T = 200 °C, which suggests that the quantum yield of luminescence increases.

The products of thermal and UV-induced decomposition of LDHs with intercalated $Pb(S_2O_3)_2^{2-}$ ions were studied by HRTEM.[290] A detailed study showed (Fig. 30)[290] that the PbS nanoparticles in the sample synthesised by UV photolysis have an amorphous shell, whereas those in the sample obtained by thermal

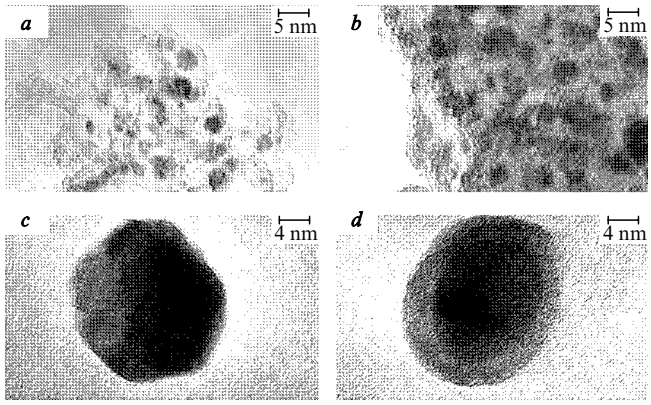


Figure 30. High-resolution electron photomicrographs of PbS particles in an LDH matrix obtained by thermal decomposition at 200 °C (*a*) and by decomposition under UV irradiation (*b*) (*c*, *d* are detailed photomicrographs of the largest particles).[290]

¶ It should be noted that in this case, the layered structure of the LDH affects the formation of semiconducting nanoparticles much more strongly than in the case where magnetic nanocomposites are synthesised by reduction at much higher temperatures than the destruction temperature of the LDH structure.

decomposition at 200 °C do not have such a shell. It is believed that the shell consists of amorphous sulfur that results from the UV-induced decomposition of the thiosulfate complex at low temperature; the absence of a similar shell in the sample obtained by thermal treatment is explained by the melting of elementary sulfur (m.p. = 119 °C). Most probably, the fact that nanoparticles of lead sulfide have an amorphous shell explains the appearance of exciton transitions in the absorption spectra and the increase in the photoluminescence intensity.

It should be noted that the optical properties of semiconducting nanoparticles depend not only on their composition, structure and size but also on the condition of the surface. It was shown that many defects on nanoparticle surfaces (*e.g.*, adsorbed atoms or structural point defects) can serve as potential holes or barriers for holes and electrons.[15] As a result, a change in the band structure and degradation of the optical properties of the nanosystem occur; the smaller the particles the more sensitive these changes to defects. In order to prevent such changes, passivation is used that makes it possible to bind the surface atoms with some other compound having a wider band gap.[297, 298] In other words, the particles are coated with a layer of an inert compound to give the so-called 'core–shell' nanoparticles. This improves considerably the optical properties of nanoparticles; as a result, these properties approach those of isolated nanoclusters.

The passivation effect is especially pronounced in luminescent properties of nanosystems.[299] In fact, the quantum yield of luminescence for coated nanoparticles of cadmium sulfide or selenide is considerably increased (almost by an order of magnitude) in comparison with free nanoparticles.[300, 301] According to literature data, the synthesis of nanoparticles in a shell is rather a complex multistage task. However, the authors succeeded in performing a one-stage synthesis of nanoparticles in a shell using anion-substituted LDHs. The interest in 'core–shell' systems is primarily related to the fact that the presence of a shell of a semiconductor with a large band gap or a dielectric results in the 'healing' of the majority of surface defects and an abrupt increase in the quantum yield of luminescence. Therefore, nanoparticles in shells show promise for creating lasers based on quantum points with adjustable wavelength and high generated power.

Yet another specific feature of LDHs is that destruction of the layered structure into separate hydroxide layers is possible. In fact, in the reaction of a dodecylsulfate-substituted Zn-Al-LDH $\{Zn_{0.67}Al_{0.33}(OH)_2[(C_{12}H_{25}SO_4)_{0.33}\cdot 2.1\,H_2O]\}$ with butanol at 120 °C, the layered structure is destructed in 24 h to give a colloid solution [302, 303] in which separate hydroxide layers are surrounded by surfactant molecules. Shaking this solution with aqueous solutions of salts results in sedimentation and recovery of the layered structure of the LDH (restructuring of the layered structure). In this case, solution anions are incorporated in the interlayer space. Hibino and Jones [304] described the destruction of the layered structure of an Mg-Al-LDH, which contained glycine anions in the interlayer space, on treatment with formamide. It was noted that the process occurred rather quickly even at room temperature.

A study of the reversible LDH for a pre-destructured sample of $Mg_2Al(OH)_6[(C_{12}H_{25}SO_4)\cdot m\,H_2O]$ showed that total recovery of the layered structure of the destructured LDH sample occurred in water and in aqueous solutions.

The reversible destruction of LDH into hydroxide layers may turn out to be rather promising for synthesising nanocomposite particles. It can be assumed that restructuring of a colloid solution of LDH layers in the presence of nanoparticles would result in the incorporation of the latter into the interlayer space of the LDH. In fact, the reaction of a colloid solution of a dodecylsulfate-substituted LDH in chloroform with a PbS sol gave a PbS/LDH nanocomposite.[289] The PbS particles formed in the matrix of the layered double hydroxide have sizes of 3–8 nm. The considerable broadening of the (00*l*) reflexes of the LDH and the low intensity of other reflexes suggest a violation of the mutual arrangement of the hydroxide layers due to intercalation of the PbS nanoparticles into the interlayer space. The accessibility of the starting reagents, the simplicity and cheapness of the synthesis, the facility of controlling the quantitative composition of the intermediates and final products and the possibility of incorporating various anions into the LDH structure make this method very promising for the synthesis of virtually any class of functional nanocomposites.

* * *

It should be noted in conclusion that utilisation of nanoreactors opens up rich possibilities for designing functional nanomaterials with predefined physicochemical characteristics that can find use in various fields of science and technology (*e.g.*, magnetic data storage devices, electronic devices, sensors, catalysts, membrane materials, *etc.*). A solid-state matrix makes it possible to avoid the aggregation of nanoparticles and protect them from external exposures, which facilitates considerably the application of such materials.

This review was financially supported in part by the Russian Foundation for Basic Research (Project No. 03-03-32182) and the programme for the State support of the leading scientific schools of the RF (Project NSh-2033.2003.3).

References

1. R W Siegel, E Hu, M C Roco (Eds) *Nanostructure Science and Technology: a Worldwide Study* (Washington, DC: NSTC, 2001)
2. A I Gusev, A A Rempel' *Nanokristallicheskie Materialy* (Nanocrystalline Materials) (Moscow: Fizmatlit, 2000)
3. M C Roco (Ed.) *Nanotechnology: Shaping the World Atom by Atom* (Washington, DC: American Chemical Society, 2000)
4. A S Edelstein, R S Cammarata (Eds) *Nanomaterials: Synthesis, Properties and Applications* (Bristol: Institute of Physics, 1998)
5. M Rieth, W Schommers, S Baskoutas *Mod. Phys. Lett. B* **14** 621 (2000)
6. I P Suzdalev, P I Suzdalev *Usp. Khim.* **70** 203 (2001) [*Russ. Chem. Rev.* **70** 177 (2001)]
7. K E Drexler *Nanosystems, Molecular Machinery, Manufacturing, and Computation* (New York: Wiley-Interscience, 1992)
8. R A Andrievskii, A M Glezer *Fiz. Met. Metalloved.* **89** 91 (2000) [a]
9. C Suryanarayana *Bull. Mater. Sci.* **17** 307 (1994)
10. R W Siegel, in *Springer Series in Materials Sciences* (Ed. F E Fujita) (Berlin: Springer, 1994) p. 65
11. P Moriarty *Rep. Prog. Phys.* **64** 297 (2001)
12. A D Pomogailo, A S Rozenberg, I E Uflyand *Nanochastitsy Metallov v Polimerakh* (Nanoparticles of Metals in Polymers) (Moscow: Khimiya, 2000)
13. C Suryanarayana, C C Koch *Hyperfine Interact.* **130** 5 (2000)
14. Y Kawazoe *Clusters and Nanomaterials: Theory and Experiment*. (Berlin: Springer, 2001)
15. A D Yoffe *Adv. Phys.* **50** 1 (2001)
16. P Marin, A Hernando *J. Magn. Magn. Mater.* **215** 729 (2000)
17. M Nogami, in *Sol-Gel Optics, Processing and Applications* (Ed. L C Klein) (Dordrecht: Kluwer Academic, 1994) p. 329
18. J H Fendler, I Dekany (Eds) *Nanoparticles in Solids and Solutions* (Dordrecht: Kluwer Academic, 1996)
19. J Lu, H Yang, S Yu, G Zou *Mater. Chem. Phys.* **45** 197 (1996)
20. P V Ananthapadmanabhan, K P Sreekumar, N Venkatramani, P K Sinha, P R Taylor *J. Alloys Compd.* **244** 70 (1996)
21. S R Shinde, A G Banpurkar, K P Adhi, A V Limaye , S B Ogale, S K Date, G Marest *Mod. Phys. Lett. B* **10** 1517 (1996)
22. A A Menovsky, J P Liu, H J Gelders, B J Harrison, H Ellermeyer, Y K Huang *Mater. Sci. Eng. A, Struct. Mater. Prop., Microstruct. Process.* **217** 227 (1996)
23. S BeginColin, F Wolf, G LeCaer *J. Phys. III* **7** 473 (1997)
24. B D Summ, N I Ivanova *Usp. Khim.* **69** 995 (2000) [*Russ. Chem. Rev.* **69** 911 (2000)]
25. J H Fendler *Chem. Mater.* **8** 1616 (1996)

26. P Vaqueiro, M A López-Quintela, J Rivas *J. Mater. Chem.* **7** 501 (1997)
27. M P Pileni, N Moumen, I Lisiecki, P Bonville, P Veilett, in *Nanoparticles in Solids and Solutions* (Eds J H Fendler, I Dekany) (Dordrecht: Kluwer Academic, 2002)
28. I Dekany, in *Nanoparticles in Solids and Solutions* (Eds J H Fendler, I Dekany) (Dordrecht: Kluwer Academic, 1996) p. 293
29. I Dekany, L Turi, G Vanko, G Lukasz, A Vertes, K Burger, in *Nanoparticles in Solids and Solutions* (Eds J H Fendler, I Dekany) (Dordrecht: Kluwer Academic, 1996) p. 555
30. N K Raman, M T Anderson, C J Brinker *Chem. Mater.* **8** 1682 (1996)
31. R S Kane, R E Cohen, R Silbey *Chem. Mater.* **8** 1919 (1996)
32. J H Fendler, F C Meldrum *Adv. Mater.* **7** 607 (1995)
33. R K Jain, R C Lind *J. Opt. Soc. Am. B* **73** 647 (1983)
34. K S Min, K V Shcheglov, C M Yang, H A Atwater, M L Brongersma, A Polman *Appl. Phys. Lett.* **68** 2511 (1996)
35. S V Kalinin, A V Lukashin, K V Tomashevich, A V Knot'ko, M P Nikiforov, S Yu Stefanovich, A A Vertegel, Yu D Tretyakov *Dokl. Akad. Nauk* **364** 207 (1999) [b]
36. S V Kalinin, A V Lukashin, M P Nikiforov, A A Eliseev, A A Vertegel, Yu D Tretyakov *Dokl. Akad. Nauk* **363** 777 (1998) [b]
37. E Cordoncillo, P Escribano, G Monros, M A Tena, V Orera, J Carda *J. Solid State Chem.* **118** 1 (1995)
38. M Nogami, Y Abe *Appl. Phys. Lett.* **65** 2545 (1994)
39. G De, L Tapfer, M Catalano, G Battaglin, F Caccavale, F Gonella, P Mazzoldi, R F Haglund Jr *Appl. Phys. Lett.* **68** 3820 (1996)
40. K Kang, A D Kepner, Y Z Hu, S W Kosh, N Peyghambarian, C-Y Li, T Takada, Y Kao, J D Mackenzie *Appl. Phys. Lett.* **64** 1487 (1994)
41. J Butty, N Peyghambarian, Y H Kao, J D Mackenzie *Appl. Phys. Lett.* **69** 3224 (1996)
42. J Butty, Y Z Hu, N Peyghambarian, Y H Kao, J D Mackenzie *Appl. Phys. Lett.* **67** 2672 (1995)
43. X H Jin, L Gao *J. Inorg. Mater.* **16** 200 (2001)
44. D Donescu *Mater. Plast.* **38** 3 (2001)
45. W Caseri *Macromol. Rapid Commun.* **21** 705 (2000)
46. P Gomez-Romero *Adv. Mater.* **13** 163 (2001)
47. A Huczko *Appl. Phys. A: Mater. Sci. Process.* **70** 365 (2000)
48. L Bronstein, E Krämer, B Berton, C Burger, S Förster, M Antonietti *Chem. Mater.* **11** 1402 (1999)
49. A A Eliseev, A V Lukashin, A A Vertegel, L I Heifets, A I Zhirov, Y D Tretyakov *Mater. Res. Innovat.* **3** 308 (2000)
50. P L J Gunter, J W Niemantsverdriet, F H Ribeiro, G A Somorjai *Catal. Rev. Sci. Eng.* **39** 77 (1997)
51. G Dantsin, K S Suslick *J. Am. Chem. Soc.* **122** 5214 (2000)
52. K W Gallis, C C Landry *Adv. Mater.* **13** 23 (2001)
53. D W Kim, A Blumstein, M Downey, J Kumar, S K Tripathy *Abstr. Pap. Am. Chem. Soc.* **220** 84 (2000)
54. N Herron *J. Inclusion Phenom. Mol. Recognit. Chem.* **21** 283 (1995)
55. J C Maxwell-Garnett *Philos. Trans. R. Soc. London* **203** 385 (1904)
56. K F Kelton *Int. J. Non-Eq. Process.* **11** 141 (1998)
57. H Sato, T Umeda *Mater. Trans., JIM* **34** 76 (1993)
58. S Komarneni *J. Sol-Gel Sci. Tech.* **6** 127 (1996)
59. H J Fecht *Mater. Trans., JIM* **36** 777 (1995)
60. B G Potter Jr, J H Simmons *Phys. Rev. B* **37** 10 838 (1988)
61. R L Comstock *J. Mater. Sci. Mater. Electron.* **13** 509 (2002)
62. A Morisako, T Naka, K Ito, U Takizawa, M Matsumoto, Y K Hong *J. Magn. Magn. Mater.* **242** 304 (2002)
63. S B Sohn, S Y Choi, I B Shim *J. Magn. Magn. Mater.* **239** 533 (2002)
64. R Müller, C Ulbrich, W Schuppel, H Steinmetz, E Steinbeiss *J. Eur. Ceram. Soc.* **19** 1547 (1999)
65. C K Lee, R F Speyer *J. Mater. Sci.* **29** 1348 (1994)
66. Yu D Tretyakov *Usp. Khim.* **72** 731 (2003) [*Russ. Chem. Rev.* **72** 651 (2003)]
67. G Ihlein, B Junges, U Junges, F Laeri, F Schuth, U Vietze *Appl. Organomet. Chem.* **12** 305 (1998)
68. A S Kovalenko, V G Il'in, O P Filippov *Teor. Eksp. Khim.* **33** 322 (1997) [c]
69. T J Pinnavaia *Adv. Chem. Ser. Mater. Chem.* **245** 283 (1995)
70. D Horváth, M Polisset-Thfoin, J Fraissard, L Guczi *Solid State Ionics* **141** 153 (2001)
71. A Fukuoka, N Higashimoto, Y Sakamoto, M Sasaki, N Sugimoto, S Inagaki, Y Fukushima, M Ichikawa *Catal. Today* **66** 23 (2001)
72. A A Kubasov *Tseolity — Kipyashchie Kamni* (Zeolites are Boiling Stones) (Moscow: Khimiya, 1998)
73. R Fricke, H Kosslick, G Lischke, M Richter *Chem. Rev.* **100** 2303 (2000)
74. K G Ione, L A Vostrikova *Usp. Khim.* **56** 393 (1987) [*Russ. Chem. Rev.* **56** 231 (1987)]
75. S Qui, R Ohnishi, M Ichikawa *J. Chem. Soc., Chem. Commun.* 1425 (1992)
76. A Carlsson, G Karlsson, J O Bovin, T Oku, Y Okamoto, N Ohnishi, O Terasaki *Eur. Phys. J. D* **9** 623 (1999)
77. Y Yamamoto, T Matsuzaki, S Tanaka, K Nishihira, K Ohdan, A Nakamura, Y Okamoto *J. Chem. Soc., Faraday Trans.* **93** 3721 (1997)
78. F J Lázaro, J L Garcia, V Schünemann, Ch Butzlaff, A Larrea, M A Zaluska-Kotur *Phys. Rev. B* **53** 13934 (1996)
79. Y M Kang, B Z Wan *Catal. Today* **35** 379 (1997)
80. D Guillemot, M Polisset-Thfoin, J Fraissard *Catal. Lett.* **41** 143 (1996)
81. Y M Kang, B Z Wan *Catal. Today* **26** 59 (1995)
82. Y M Kang, B Z Wan *Appl. Catal., A* **128** 53 (1995)
83. F E Trigueiro, D F J Monteiro, F M Z Zotin, E F Sousa-Aguiar *J. Alloys Compd.* **344** 337 (2002)
84. P W de Bont, M J Vissenberg, E J M Hensen, V H J de Beer, J A R van Veen, R A van Santen, A M van der Kraan *Appl. Catal., A* **236** 205 (2002)
85. P W de Bont, M J Vissenberg, E Boellaard, V H J de Beer, J A R van Veen, R A van Santen, A M van der Kraan *Hyperfine Interact.* **111** 39 (1998)
86. A Seidel, J Loos, B Boddenberg *J. Mater. Chem.* **9** 2495 (1999)
87. N Nishimiya, T Kishi, T Mizushima, A Matsumoto, K Tsutsumi *J. Alloys Compd.* **319** 312 (2001)
88. T Rades, M Polisset-Thfoin, J Fraissard *Top. Catal.* **11** 283 (2000)
89. A M Diamy, Z Randriamanantenasoa, J C Legrand, M PolissetThfoin, J Fraissard *Chem. Phys. Lett.* **269** 327 (1997)
90. Y Okamoto, H Kikuta, Y Ohto, S Nasu, O Terasaki, in *Progress in Zeolite and Microporous Materials. Studies in Surface Science and Catalysis* (Amsterdam: Elsevier, 1997) p. 2051
91. T M Salama, R Ohnishi, T Shido, M Ichikawa *J. Catal.* **162** 169 (1996)
92. T M Salama, T Shido, H Minagawa, M Ichikawa *J. Catal.* **152** 322 (1995)
93. H V Garcia, M H Velez, O S Garrido, J M M Duart, J Jimenez *Solid-State Electron.* **43** 1171 (1999)
94. G G Lindner, K Witke, H Schlaich, D Reinen *Inorg. Chim. Acta* **252** 39 (1996)
95. J F Jia, K S Pillai, W M H Sachtler *J. Catal.* **221** 119 (2004)
96. A Z Abdullah, M Z Abu Bakar, S Bhatia *Catal. Commun.* **4** 555 (2003)
97. J Perez-Ramirez, G Mul, F Kapteijn, J A Moulijn, A R Overweg, A Domenech, A Ribera, I W C E Arends *J. Catal.* **207** 113 (2002)
98. X T Li, C L Shao, S L Qiu, F S Xiao, W T Zheng, P L Ying, O Terasaki *Microporous Mesoporous Mater.* **40** 263 (2000)
99. X T Li, C L Shao, S L Qiu, F S Siao, W T Zheng, Z M Liu, O M Terasaki *Mater. Lett.* **48** 242 (2001)
100. Z J Li, M Flytzani-Stephanopoulos *J. Catal.* **182** 313 (1999)
101. J S Beck, J C Vartuli, W J Roth, M E Leonowicz, C T Kresge, K D Shmitt, C T W Chu, D H Olson , E W Sheppard, S B McCullen, J B Higgins, J L Schlenker *J. Am. Chem. Soc.* **114** 10 834 (1992)
102. Y Wei, D L Jin, T Z Ding, W H Shih, X H Liu, S Z D Cheng, Q Fu *Adv. Mater.* **10** 313 (1998)
103. S Sakka *Am. Ceram. Soc. Bull.* **64** 1463 (1985)
104. D Y Zhao, J L Feng, Q S Huo, N Melosh, G H Fredrickson, B F Chmelka, G D Stucky *Science* **279** 548 (1998)
105. A A Eliseev, A V Lukashin, L I Soboleva, A V Knot'ko, L I Kheifets, A A Vertegel, Yu D Tretyakov *Dokl. Akad. Nauk* **372** 770 (2000) [b]

106. L I Soboleva, A A Eliseev, A V Lukashin, A A Vertegel, Yu D Tretyakov *Vestn. Voronezh. GTU, Ser. Materialoved.* **1.8** 16 (2000)
107. H O Pastore, M Munsignatti, D R S Bittencourt, M M Rippel *Microporous Mesoporous Mater.* **32** 211 (1999)
108. J C Vartuli, K D Schmitt, C T Kresge, W J Roth , M E Leonowicz, S B McCullen, S D Hellring, J S Beck , J L Schlenker, D H Olson, E W Sheppard *Chem. Mater.* **6** 2317 (1994)
109. Z Gabelica, J M Clacens, R Sobry, G VandenBossche *Characterization of Hexagonal and Lamellar Mesoporous Silicas, Alumino- and Gallosilicates by Small-Angle X-Ray Scattering (SAXS) and Multinuclear Solid State NMR* (Amsterdam: Elsevier, 1995)
110. P T Tanev, Y Liang, T J Pinnavaia *J. Am. Chem. Soc.* **119** 8616 (1997)
111. Z T Zhang, Y Han, F S Xiao, S L Qiu, L Zhu, R W Wang, Y Yu, Z Zhang, B S Zou, Y Q Wang, H P Sun, D Y Zhao, Y Wei *J. Am. Chem. Soc.* **123** 5014 (2001)
112. T J Barton, L M Bull, W G Klemperer, D A Loy, B McEnaney, M Misono, P A Monson, G Pez, G W Scherer, J C Vartuli, O M Yaghi *Chem. Mater.* **11** 2633 (1999)
113. C F Cheng, D H Park, J Klinowski *J. Chem. Soc., Faraday Trans.* **93** 193 (1997)
114. F Quirion, L Magid *J. Phys. Chem.* **90** 5435 (1986)
115. P T Tanev, T J Pinnavaia *Science* **267** 865 (1995)
116. P Schmidt-Winkel, C J Glinka, G D Stucky *Langmuir* **16** 356 (2000)
117. M Kruk, M Jaroniec, A Sayari *Langmuir* **13** 6267 (1997)
118. C T Kresge, M E Leonowicz, W J Roth, J C Vartuli *Nature (London)* **359** 710 (1992)
119. H Miyata, K Kuroda *J. Am. Chem. Soc.* **121** 7618 (1999)
120. H Yang, A Kuperman, N Coombs, S MamicheAfara, G A Ozin *Nature (London)* **379** 703 (1996)
121. H Yang, N Coombs, I Sokolov, G A Ozin *J. Mater. Chem.* **7** 1285 (1997)
122. A Corma, V Fornes, M T Navarro, J Perez-Pariente *J. Catal.* **148** 569 (1994)
123. F Schuth *Ber. Bunsen.-Ges. Phys. Chem.* **99** 1306 (1995)
124. G-G Wu, T Bien *Science* **264** 1757 (1994)
125. G-G Wu, T Bien *Science* **266** 1013 (1994)
126. A Corma, V Fornes, H Garcia, M A Miranda, M J Sabater *J. Am. Chem. Soc.* **116** 9767 (1994)
127. US P. 5 364 797 (1994)
128. M J MacLachlan, P Aroca, N Coombs, I Manners, G A Ozin *Adv. Mater.* **10** 144 (1998)
129. R Leon, D Margolese, G D Stucky, P M Petroff *Phys. Rev. B* **52** 2285 (1995)
130. C Jinwoo, K Lee, H Kang, S L Oh, H-C Ri *Mater. Res. Soc. Symp. Proc.* **635** C. 3.3.1. (2001)
131. H Parala, H Winkler, M Kolbe, A Wohlfart, R A Fischer, R Schmechel, H von Seggern *Adv. Mater.* **12** 1050 (2000)
132. K S Napolskii, I V Kolesnik, A A Eliseev, A V Lukashin, A A Vertegel, Yu D Tretyakov *Dokl. Akad. Nauk* **386** 207 (2002) [b]
133. K S Napolskii, A A Eliseev, A V Knot'ko, A V Lukashin, A A Vertegel, Yu D Tretyakov *Vestn. Voronezh. GTU, Ser. Materialoved.* **1.11** 3 (2002)
134. A A Eliseev, K S Napolskii, A V Lukashin, Y D Tretyakov *J. Magn. Magn. Mater.* **272** (2004) (in the press)
135. E A Kelberg, S V Grigoriev, A I Okorokov, H Eckerlebe, N A Grigorieva, A A Eliseev, A V Lukashin, A A Vertegel, K S Napolskii *Physica B* **350** e305 (2004)
136. S V Grigoriev, A I Okorokov, H Eckerlebe, N A Grigorieva, A A Eliseev, A V Lukashin, K S Napolskii *Physica E* (2004) (in the press)
137. E A Kelberg, S V Grigoriev, A I Okorokov, H Eckerlebe, N A Grigorieva, W H Kraan, A A Eliseev, A V Lukashin, A A Vertegel, K S Napolskii *Physica B* **335** 123 (2003)
138. W-H Zhang, J-L Shi, L-Z Wang, D-S Yan *Chem. Mater.* **12** 1408 (2000)
139. R P Cowburn, D K Koltsov, A O Adeyeye, M E Welland *Europhys. Lett.* **48** 221 (1999)
140. A A Eliseev, K S Napolskii, D F Gorozhankin, A V Lukashin, Y D Tretyakov, N A Grigorieva, S V Grigoriev, A A Vorobiev, P Goernert *Mater. Res. Soc. Symp. Proc.* L.6.1 (2003)
141. A A Eliseev, K S Napolskii, A V Lukashin, Y D Tretyakov, in *Proceedings of the 13th NID Workshop, Athens, Greece, 2004* p. 77
142. M Sasaki, M Osada, N Sugimoto, S Inagaki, Y Fukushima, A Fukuoka, M Ichikawa *Microporous Mesoporous Mater.* **21** 597 (1998)
143. M Sasaki, M Osada, N Higashimoto, T Yamamoto, A Fukuoka, M Ichikawa *J. Mol. Catal. A: Chem.* **141** 223 (1999)
144. I V Kolesnik, A A Eliseev, A P Malakho, A V Garshev, V P Tarasov, A V Lukashin, Yu D Tretyakov *Dokl. Akad. Nauk* **396** (2004) [b] (in the press)
145. A A Eliseev, K S Napolskii, I V Kolesnik, Yu V Kolenko, A V Lukashin, P Goernert, Y D Tretyakov, in *Frontiers in Molecular Science and Technology of Nanocarbon, Nanosilicon and Biopolymer Integrated Nanosystems* (Eds E V Buzaneva, P Scharff) (Dordrecht: Kluwer Academic, 2004)
146. A A Eliseev, S V Kalinin, V I Privalov, A A Vertegel, Y D Tretyakov *J. Solid State Chem.* **147** 304 (1999)
147. S Shingubara *J. Nanoparticle Res.* **5** 17 (2003)
148. F Keller, M S Hunter, D L Robinson *J. Electrochem. Soc.* **100** 411 (1953)
149. T P Hoar, N F Mott *J. Phys. Chem. Solids* **9** 97 (1959)
150. J P O'Sullivan, G C Wood *Proc. R. Soc. London, Ser. A* **317** 511 (1970)
151. G E Thompson, R C Furneaux, G C Wood, J A Richardson, J S Goode *Nature (London)* **272** 433 (1978)
152. O Jessensky, F Muüler, U Gösele *J. Electrochem. Soc.* **145** 3735 (1998)
153. O Jessensky, F Müller, U Gösele *Appl. Phys. Lett.* **72** 1173 (1998)
154. K Nielsch, J Choi, K Schwirn, R B Wehrspohn, U Gösele *Nano Lett.* **2** 677 (2002)
155. H Masuda, K Fukuda *Science* **268** 1466 (1995)
156. G C Schwartz, V Platter *J. Electrochem. Soc.* **122** 1508 (1975)
157. S Shingubara, O Okino, Y Sayama, H Sakaue, T Takahagi *Jpn. J. Appl. Phys.* **36** 7791 (1997)
158. H Masuda, F Hasegwa, S Ono *J. Electrochem. Soc.* **144** L127 (1997)
159. H Masuda, K Yada, A Osaka *Jpn. J. Appl. Phys. Lett.* **37** L1340 (1998)
160. H Masuda, H Yamada, M Satoh, H Asoh, M Nakao, T Tamamura *Appl. Phys. Lett.* **71** 2770 (1997)
161. H Asoh, K Nishio, M Nakao, A Yokoo, T Tamamura, H Masuda *J. Vac. Sci. Technol., B* **19** 569 (2001)
162. S Shingubara, Y Murakami, K Morimoto, T Takahagi *Surf. Sci.* **532** 317 (2003)
163. J Y Liang, H Chik, A J Yin, J Xu *J. Appl. Phys.* **91** 2544 (2002)
164. L Chen, A J Yin, J S Im, A V Nurmikko, J M Xu, J Han *Phys. Status Solidi A* **188** 135 (2001)
165. M Nakao, S Oku, T Tamamura, K Yasui, H Masuda *Jpn. J. Appl. Phys.* **38** 1052 (1999)
166. T Kawai, S I Ishiguro, H Ohtaki *Bull. Chem. Soc. Jpn.* **53** 2221 (1980)
167. S Kawai, I Ishiguro *J. Electrochem. Soc.* **123** 1047 (1976)
168. R Ueda, S Kawai, I Ishiguro *J. Vac. Sci. Technol.* **12** 759 (1975)
169. S H Sun, C B Murray, D Weller, L Folks, A Moser *Science* **287** 1989 (2000)
170. S H Sun, E E Fullerton, D Weller, C B Murray *IEEE Trans. Magn.* **37** 1239 (2001)
171. K Nielsch, F Muller, A P Li, U Gosele *Adv. Mater.* **12** 582 (2000)
172. M Krlll, W J Blau, D Grandjean, R E Benfield, F Luis, P M Paulus, L J de Jongh *J. Magn. Magn. Mater.* **249** 241 (2002)
173. H Zeng, R Skomski, L Menon, Y Liu, S Bandyopadhyay, D J Sellmyer *Phys. Rev. B* **65** 4426 (2002)
174. H Zeng, S Michalski, R D Kirby, D J Sellmyer, L Menon, S Bandyopadhyay *J. Phys.: Condens. Matter* **14** 715 (2002)
175. P M Paulus, F Luis, M Kroll, G Schmid, L J de Jongh *J. Magn. Magn. Mater.* **224** 180 (2001)

176. M Zheng, L Menon, H Zeng, Y Liu, S Bandyopadhyay, R D Kirby, D J Sellmyer *Phys. Rev. B* **62** 12 282 (2000)
177. L Menon, M Zheng, H Zeng, S Bandyopadhyay, D J Sellmyer *J. Electron. Mater.* **29** 510 (2000)
178. R M Metzger, V V Konovalov, M Sun, T Xu, G Zangari, B Xu, M Benakli, W D Doyle *IEEE Trans. Magn.* **36** 30 (2000)
179. M Sun, G Zangari, R M Metzger *IEEE Trans. Magn.* **36** 3005 (2000)
180. H Zeng, M Zheng, R Skomski, D J Sellmyer, Y Liu, L Menon, S Bandyopadhyay *J. Appl. Phys.* **87** 4718 (2000)
181. G J Strijkers, J H J Dalderop, M A A Broeksteeg, H J M Swagten, W J M de Jonge *J. Appl. Phys.* **86** 5141 (1999)
182. L Menon, S Bandyopadhyay, Y Liu, H Zeng, D J Sellmyer *J. Nanosci. Nanotechnol.* **1** 149 (2001)
183. H Zhu, S G Yang, G Ni, D L Yu, Y W Du *Scr. Mater.* **44** 2291 (2001)
184. A V Kukhta, G G Gorokh, E E Kolesnik, A I Mitkovets, M I Taoubi, Y A Koshin, A M Mozalev *Surf. Sci.* **507** 593 (2002)
185. Y Du, W L Cai, C M Mo, J Chen, L D Zhang, X G Zhu *Appl. Phys. Lett.* **74** 2951 (1999)
186. G Shi, C M Mo, W L Cai, L D Zhang *Solid State Commun.* **115** 253 (2000)
187. Y H Wang, Y Q Xu, W L Cai, J M Mo *Acta Phys.-Chim. Sinica* **18** 943 (2002)
188. O Rabin, P R Herz, S B Cronin, Y Lin, A I Akinwande, M S Dresselhaus *Mater. Res. Soc. Symp. Proc.* **636** D. 4.7.1 (2001)
189. N V Gaponenko, O V Sergeev, E A Stepanova, V M Parkun, A V Mudryi, H Gnaser, J Misiewicz, R Heiderhoff, L J Balk, G E Thompson *J. Electrochem. Soc.* **148** H13 (2001)
190. N V Gaponenko, J A Davidson, B Hamilton, P Skeldon, G E Thompson, X Zhou, J C Pivin *Appl. Phys. Lett.* **76** 1006 (2000)
191. G S Cheng, L D Zhang, X G Zhu, S H Chen, Y Li, Y Zhu, G T Fei *Nanostruct. Mater.* **11** 421 (1999)
192. C X Xu, Q H Xue, Y Zhong, Y P Cui, L Ba, B Zhao, N Gu *Nanotechnology* **13** 47 (2002)
193. I Mikulskas, S Juodkazis, A Jagminas, S Meskinis, J G Dumas, J Vaitkus, R Tomasiunas *Opt. Mater.* **17** 343 (2001)
194. I Mikulskas, S Juodkazis, R Tomasiunas, J G Dumas *Adv. Mater.* **13** 1574 (2001)
195. R B Wehrspohn, J Schilling *MRS Bull.* **26** 623 (2001)
196. H Masuda, M Ohya, K Nishio, H Asoh, M Nakao, M Nohtomi, A Yokoo, T Tamamura *Jpn. J. Appl. Phys. Lett.* **39** L1039 (2000)
197. H Masuda, M Ohya, H Asoh, M Nakao, M Nohtomi, T Tamamura *Jpn. J. Appl. Phys. Lett.* **38** L1403 (1999)
198. T Iwasaki, T Motoi, T Den *Appl. Phys. Lett.* **75** 2044 (1999)
199. J Li, C Papadopoulos, J M Xu, M Moskovits *Appl. Phys. Lett.* **75** 367 (1999)
200. S L Sung, S H Tsai, C H Tseng, F K Chiang, X W Liu, H C Shih *Appl. Phys. Lett.* **74** 197 (1999)
201. S L Sung, S H Tsai, X W Liu, H C Shih *J. Mater. Res.* **15** 502 (2000)
202. J Li, C Papadopoulos, J Xu *Nature (London)* **402** 253 (1999)
203. X H Wang, Z Hu, Q Wu, Y Chen *Catal. Today* **72** 205 (2002)
204. Y C Sui, B Z Cui, R Guardian, D R Acosta, L Martinez, R Perez *Carbon* **40** 1011 (2002)
205. W C Hu, L M Yuan, Z Chen, D W Gong, K Saito *J. Nanosci. Nanotechnol.* **2** 203 (2002)
206. A Mozalev, S Magaino, H Imai *Electrochim. Acta* **46** 2825 (2001)
207. E A Bluhm, E Bauer, R M Chamberlin, K D Abney, J S Young, G D Jarvinen *Langmuir* **15** 8668 (1999)
208. E A Bluhm, N C Schroeder, E Bauer, J N Fife, R M Chamberlin, K D Abney, J S Young, G D Jarvinen *Langmuir* **16** 7056 (2000)
209. A T Shawaqfeh, R E Baltus *J. Membr. Sci.* **157** 147 (1999)
210. S Basu, S Chatterjee, M Saha, S Bandyopadhay, K K Mistry, K Sengupta *Sens. Actuators, B* **79** 182 (2001)
211. R Schöllhorn *Chem. Mater.* **8** 1747 (1996)
212. S Carlino *Chem. Br.* **33** 59 (1997)
213. T Sato, Y Fukugami, Y Shu *Scr. Mater.* **44** 1905 (2001)
214. J J Tunney, C Detellier *Chem. Mater.* **8** 927 (1996)
215. A S Zerda, A J Lesser *J. Polym. Sci., Part B: Polym. Phys.* **39** 1137 (2001)
216. D W Kim, A Blumstein, J Kumar, S K Tripathy *Chem. Mater.* **13** 243 (2001)
217. A Szucs, F Berger, I Dekany *Colloid Surf., A* **174** 387 (2000)
218. H R Fischer, L H Gielgens, T P M Koster *Acta Polym.* **50** 122 (1999)
219. T Sato, K Masaki, K I Sato, Y Fujishiro, A Okuwaki *J. Chem. Technol. Biotechnol.* **67** 339 (1996)
220. E P Giannelis *Appl. Organomet. Chem.* **12** 675 (1998)
221. Y Ma, W Tong, H Zhou, S L Suib *Microporous Mesoporous Mater.* **37** 243 (2000)
222. F Cavani, F Trifiro, A Vaccari *Catal. Today* **11** 173 (1991)
223. F Trifiro, A Vaccari, in *Comprehensive Supramolecular Chemistry* Vol. 7 (Eds J L Atwood, J E D Davies, D D MacNicol, F Vogtle, J M Lehn, G Alberti, T Beins) (Oxford: Pergamon Press, 1996)
224. F Basile, L Basini, G Fornasari, M Gazzano, F Trifiro, A Vaccari *Stud. Surf. Sci. Catal.* **118** 31 (1998)
225. C Barriga, J M Fernandez, M A Ulibarri, F M Labajos, V Rives *J. Solid State Chem.* **124** 205 (1996)
226. J M Fernández, C Barriga, M A Ulibarri, F M Labajos, V Rives *Chem. Mater.* **9** 312 (1997)
227. F M Labajos, V Rives, P Malet, M A Centeno, M A Ulibarri *Inorg. Chem.* **35** 1154 (1996)
228. M A Aramendia, V Borau, C Jimenez, J M Marinas, F J Romero, J R Ruiz *J. Solid State Chem.* **131** 78 (1997)
229. F M Vichi, O L Alves *J. Mater. Chem.* **7** 1631 (1997)
230. M A Aramendia, V Borau, C Jiménez, J M Marinas, F J Romero, F J Urbano *J. Mater. Chem.* **9** 2291 (1999)
231. M Bellotto, B Rebours, O Clause, J Lynch, D Bazin, E Elkaim *J. Phys. Chem.* **100** 8527 (1996)
232. V Rives, M A Ulibarri *Coord. Chem. Rev.* **181** 61 (1999)
233. A Roy, C Forano, K El Malki, J P Besse, in *Synthesis of Microporous Materials* Vol. 2 (Eds M L Occelli, H E Robson) (New York: Reinhold, 1992)
234. F C Hawthorne, S V Krivovichev, P C Burns *Rev. Mineral., Geochem.* **40** 1 (2000)
235. S H Han, C G Zhang, W G Hou, D J Sun, G T Wang *Chem. J. Chin. Univ.* **17** 1785 (1996)
236. C J Serna, J L Rendon, J E Iglesias *Clays Clay Miner.* **10** 180 (1982)
237. S Velu, D P Sabde, N Shah, S Sivasanker *Chem. Mater.* **10** 3451 (1998)
238. S Velu, K Suzuki, M Okazaki, T Osaki, S Tomura, F Ohashi *Chem. Mater.* **11** 2163 (1999)
239. S Velu, C S Swamy *J. Mater. Sci. Lett.* **15** 1674 (1996)
240. H B Friedrich, F Khan, N Singh, M van Staden *Synlett* 869 (2001)
241. F Basile, G Fornasari, M Gazzano, A Vaccari *Appl. Clay Sci.* **16** 185 (2000)
242. S P Newman, W Jones *New J. Chem.* **22** 105 (1998)
243. J Evans, M Pillinger, J J Zhang *J. Chem. Soc., Dalton Trans.* 2963 (1996)
244. S K Yun, T J Pinnavaia *Inorg. Chem.* **35** 6853 (1996)
245. E A Gardner, S K Yun, T H Kwon, T J Pinnavaia *Appl. Clay Sci.* **13** 479 (1998)
246. W T Reichle *Solid State Ionics* **22** 135 (1986)
247. S P Newman, W Jones *J. Solid State Chem.* **148** 26 (1999)
248. E L Crepaldi, J B Valim *Quim. Nova* **21** 300 (1998)
249. Y Israëli, T Taviot-Guého, J P Beese, J P Morel, N Morel-Desrosiers *J. Chem. Soc., Dalton Trans.* 791 (2000)
250. M A Drezdzon *Inorg. Chem.* **27** 4628 (1988)
251. C W Hu, X Zhang, Q L He, E B Wang, S W Wang, Q L Guo *Transition Met. Chem.* **22** 197 (1997)
252. F Kooli, W Jones, V Rives, M A Ulibarri *J. Mater. Sci. Lett.* **16** 27 (1997)
253. K Chibwe, W Jones *Chem. Mater.* **1** 489 (1989)
254. K Chibwe, W Jones *J. Chem. Soc., Chem. Commun.* 926 (1989)
255. S Carlino, M J Hudson *J. Mater. Chem.* **4** 99 (1994)
256. S B C Pergher, A Corma, V Fornes *Quim. Nova* **22** 693 (1999)
257. T Okuhara, N Mizuno, M Misono *Adv. Catal.* **41** 113 (1996)

258. A Corma *Chem. Rev.* **97** 2373 (1997)
259. I V Kozhevnikov *Chem. Rev.* **98** 171 (1998)
260. D Tichit, F Medina, B Coq, R Dutartre *Appl. Catal., A* **159** 241 (1997)
261. E D Rodeghiero, J Chisaki, E P Giannelis *Chem. Mater.* **9** 478 (1997)
262. D Tichit, A Vaccari *Appl. Clay Sci.* **13** 311 (1998)
263. D Tichit, F Fajula *Stud. Surf. Sci. Catal.* **125** 329 (1999)
264. B Sels, D De Vos, M Buntinx, F Pierard, A Kirsch-De Mesmaeker, P Jacobs *Nature (London)* **400** 855 (1999)
265. L Indira, P V Kamath *J. Mater. Chem.* **4** 1487 (1994)
266. P V Kamath, M Dixit, L Indira, A K Shukla, V G Kumar, N Munichandraiah *J. Electrochem. Soc.* **141** 2956 (1994)
267. G A Caravaggio, C Detellier, Z Wronski *J. Mater. Chem.* **11** 912 (2001)
268. M Morigi, E Scavetta, M Berrettoni, M Giorgetti, D Tonelli *Anal. Chim. Acta* **439** 265 (2001)
269. R Schöllhorn, B Otto *J. Chem. Soc., Chem. Commun.* 1222 (1986)
270. B Ballarin, M Morigi, E Scavetta, R Seeber, D Tonelli *J. Electroanal. Chem.* **492** 7 (2000)
271. E Scavetta, M Berrettoni, R Seeber, D Tonelli *Electrochim. Acta* **46** 2681 (2001)
272. T Sato, H Okuyama, T Endo, M Shimada *React. Solids* **8** 63 (1990)
273. Y Fujishiro, S Uchida, T Sato *Int. J. Inorg. Mater.* **1** 67 (1999)
274. T Sato, K I Sato, Y Fujishiro, T Yoshioka, A Okuwaki *J. Chem. Technol. Biotechnol.* **67** 345 (1996)
275. T Sato, K Masaki, T Yoshioka, A Okuwaki *J. Chem. Technol. Biotechnol.* **58** 315 (1993)
276. V P Isupov, K A Tarasov, L E Chupakhina, R P Mitrofanova, V V Boldyrev *Dokl. Akad. Nauk* **336** 209 (1994) [b]
277. V P Isupov, K A Tarasov, L E Chupakhina, R P Mitrofanova, L I Skvortsova, V V Boldyrev *Zh. Neorg. Khim.* **40** 22 (1995) [d]
278. V P Isupov, L E Chupakhina, R P Mitrofanova, K A Tarasov, A Y Rogachev, V V Boldyrev *Solid State Ionics* **101** 265 (1997)
279. V P Isupov, L E Chupakhina, R P Mitrofanova, K A Tarasov *Zh. Strukt. Khim.* **12** 454 (1998) [e]
280. K A Tarasov, V P Isupov, B B Bokhonov, Y A Gaponov, B P Tolochko, M R Sharafutdinov, S S Shatskaya *J. Mater. Synth. Process.* **8** 21 (2000)
281. K A Tarasov, V P Isupov, L E Chupakhina *Zh. Neorg. Khim.* **45** 1804 (2000) [d]
282. A V Lukashin, S V Kalinin, M P Nikiforov, N G Zhuravleva, A I Zhirov, V I Privalov, A A Vertegel *Mater. Res. Soc. Symp. Proc.* **547** 239 (1999)
283. A A Eliseev, A V Lukashin, A A Vertegel, Yu D Tretyakov *Vestn. Voronezh. GTU, Ser. Materialoved.* **1.8** 6 (2000)
284. A V Lukashin, S V Kalinin, M P Nikiforov, V I Privalov, A A Eliseev, A A Vertegel, Yu D Tretyakov *Dokl. Akad. Nauk* **364** 77 (1999) [b]
285. A A Eliseev, A V Lukashin, A A Vertegel, V P Tarasov, Yu D Tretyakov *Dokl. Akad. Nauk* **387** 777 (2002) [b]
286. A V Lukashin, A A Vertegel, A A Eliseev, M P Nikiforov, P Gornert, Y D Tretyakov *J. Nanoparticle Res.* **5** 455 (2003)
287. M P Nikiforov, M V Chernysheva, A V Lukashin, A A Vertegel, Yu V Maksimov, S V Novichikhin, I P Suzdalev, Yu D Tretyakov *Dokl. Akad. Nauk* **391** 53 (2003) [b]
288. A V Lukashin, M V Chernysheva, A A Vertegel, Yu D Tretyakov *Dokl. Akad. Nauk* **388** 200 (2003) [b]
289. A V Lukashin, A S Vyacheslavov, A A Vertegel, Yu D Tretyakov *Dokl. Akad. Nauk* **385** 71 (2002) [b]
290. A V Lukashin, A A Eliseev, N G Zhuravleva, S V Kalinin, A A Vertegel, Yu D Tretyakov *Dokl. Akad. Nauk* **383** 504 (2002) [b]
291. A V Lukashin, A A Vertegel, A A Eliseev, N G Zhuravleva, M P Nikiforov, Y D Tretyakov, in *Proceedings of the VIIIth European Conference on Solid State Chemistry, Oslo, Norway, 2001* p. 21
292. A V Lukashin, S V Kalinin, S R Lee, A V Knot'ko, A A Vertegel, Y D Tretyakov *NATO ASI Ser., Ser. 2* **17** 228 (2001)
293. A V Lukashin, A A Vertegel, N G Zhuravleva, Y D Tretyakov, in *Proceedings of the 2000 MRS Fall Meeting, Boston, USA, 2000* p. 236
294. N G Zhuravleva, A A Eliseev, A V Lukashin, A A Vertegel, Yu D Tretyakov *Vestn. Voronezh. GTU, Ser. Materialoved.* **1.8** 11 (2000)
295. X C Ai, L Guo, Y H Zou, Q S Li, H S Zhu *Mater. Lett.* **38** 131 (1999)
296. A A Patel, F X Wu, J Z Zhang, C L Torres-Martinez, R K Mehra, Y Yang, S H Risbud *J. Phys. Chem. B* **104** 11 598 (2000)
297. P Mulvaney, L M Liz-Marzán, M Giersig, T Ung *J. Mater. Chem.* **10** 1259 (2000)
298. F Caruso *Adv. Mater.* **13** 11 (2001)
299. M Kuno, J K Lee, B O Dabbousi, F V Mikulec, M G Bawendi *J. Chem. Phys.* **106** 9869 (1997)
300. X G Peng, M C Schlamp, A V Kadavanich, A P Alivisatos *J. Am. Chem. Soc.* **119** 7019 (1997)
301. M Danek, K F Jensen, C B Murray, M G Bawendi *Chem. Mater.* **8** 173 (1996)
302. M Adachi-Pagano, C Forano, J P Besse *Chem. Commun.* 91 (2000)
303. F Leroux, M Adachi-Pagano, M Intissar, S Chauvizhre, C Forano, J-P Besse *J. Mater. Chem.* **11** 105 (2001)
304. T Hibino, W Jones *J. Mater. Chem.* **11** 1321 (2001)

[a] — *Phys. Met. Metallogr. (Engl. Transl.)*
[b] — *Dokl. Chem. (Engl. Transl.)*
[c] — *Theor. Exp. Chem. (Engl. Transl.)*
[d] — *Russ. J. Inorg. Chem. (Engl. Transl.)*
[e] — *Russ. J. Struct. Chem. (Engl. Transl.)*